POLITECNICO
MILANO 1863

DIPARTIMENTO DI MECCANICA

mecc

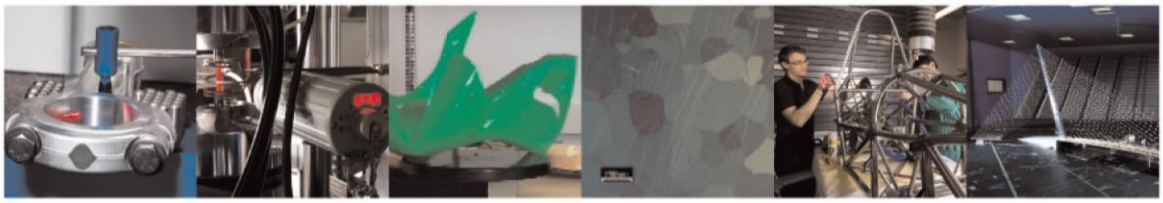

CFD and experimental analysis of the coolant flow in cryogenic milling

Tahmasebi, Ehsan; Albertelli, Paolo; Lucchini, Tommaso; Monno, Michele; Mussi, Valerio

This is a post-peer-review, pre-copyedit version of an article published in INTERNATIONAL JOURNAL OF MACHINE TOOLS & MANUFACTURE. The final authenticated version is available online at: http://dx.doi.org/10.1016/j.ijmachtools.2019.02.003

This content is provided under CC BY-NC-ND 4.0 license

DIPARTIMENTO DI MECCANICA ■ POLITECNICO DI MILANO
via G. La Masa, 1 ■ 20156 Milano ■ EMAIL (PEC): pecmecc@cert.polimi.it
http://www.mecc.polimi.it
Rev. 0

CFD and experimental analysis of the coolant flow in cryogenic milling

Abstract

Cryogenic cooling could improve the machining performance for hard-to-cut materials. Deployment of this modern technology for milling applications, specifically because of their severe working conditions and complicated physical phenomena inside cryogenic fluids, requires further research to become credible for industrial applications. Obtaining accurate models for coolant behavior is essential for optimum design, prediction of operational limits, and safe control of the cooling process. In this paper, Computational Fluid Dynamics (CFD) were used to determine the behavior of the liquid nitrogen (LN_2) inside the coolant delivery system and the interaction of the coolant jet with the cutting area. The role of working conditions as well as nozzle geometry, formation of cavitation inside the tool, coolant pressure, and wall temperature on the efficiency of the coolant delivery were investigated in this study. Initial experimental flow measurements were used to predict the simulation setup and evaluate the results. Experimental milling tests were performed to verify the numerical findings. Cutting forces, coolant mass flow rate, temperature, and pressure were measured during the tests. A mechanistic cutting force model and the morphology of the chips were used to interpret the effect of liquid nitrogen on the cutting mechanisms. Results of this study offer three main suggestions for reliable industrial cryogenic milling: using liquid nitrogen in the range of 2 to 4 bar, improving the insulation of the feeding line and finding a technical solution for non-insulated parts, and increasing the quality of the liquid in the coolant mixture close to the milling head. Outcomes of this study could help to improve the cooling performance and implement a reliable industrial solution for cryogenic milling.

1. Introduction

In machining processes work pieces and tools are exposed to a significant thermal load resulting from shearing and friction between the cutting tool and the workpiece [1][2][3]. Proper cooling reduces the tool wear and improves the machined surface quality. However, the use of cutting fluids involves additional costs, and if not properly managed, poses a health hazard to the operator. Moreover, the disposal of the exhausted cutting fluids is a challenge for sustainable manufacturing. Using cryogenic cooling could improve the machining performance for hard-to-cut materials and could solve the environmental issues [4] [5][6][7].

So far, most of the advantages of the cryogenic cooling for machining process have been scientifically tested at the laboratory scale, on pilot setups. but, to increase its technology readiness level (TRL), more studies and researches need to be developed [8][9].

Several relatively recent studies on the benefits of cryogenic cooling [10][11][12] have been found. Some of these investigated the lubrication effects of cryogenic coolant like liquid N_2 [13][14] and

liquid CO_2 [15][16][17]. Hong et al.[12] found that, due to the quick evaporation of cryogenics, they cannot provide boundary lubrication like conventional lubricants. On the contrary, the formation of a liquid/gas film between the sliding surfaces could reduce the contact area and friction forces [11]. Some researchers focused on the optimization of the cryogenic cooling strategy. For milling operations, Nalbant and Yildiz [18] designed an external jet system to spray LN_2 into the tool-workpiece interface. Biermann and Heilmann [19] designed two delivery systems suitable for face milling aluminum alloys. Several studies focused on the effects of cryogenic cooling on cutting temperatures. Shokrani et al. [20][21][22][23] studied the potentialities of cryogenic cooling for machining hard-to-cut materials (i.e. titanium-based or nickel-based alloys). According to the results of their studies, it was observed that promising improvements, concerning the expected tool life, can be expected. Focusing on the surface finishing, the best cooling approach is the one that ensures the cryogenic jet penetrating into the cutting zone.

Strano et al. [24] focused on cryogenic cooling for Ti6Al4V. Focusing on a turning application, they compared the cutting forces and tool life obtained in experiments carried out both using cryogenic and flooding cooling strategies. The researchers continued their study by considering the economic aspects of cryogenic turning [25]. In addition, they carried out some finite element analysis of the turning process with cryogenic cooling in comparison to dry cutting [26].

Although several studies on the interaction between the cryogenic coolant and the machining process can be found, there are not enough research studies related to the feeding system and on the issues that need to be tackled to guarantee a reliable and constant cryogenic coolant jet.

Providing a reliable flow of the cryogenic coolant is a key aspect for industrializing this technology. For instance, Pusavec et al. [27] focused on the cryogenic coolant efficiency. They investigated the effect of the nitrogen phase on turning machining. The team an innovative experimental setup to detect the emerging coolant phase and measured the temperature of the surface in which coolant impinged to the metal part. Their work has shown that the coolant phase and its flow rate have a significant effect on the tool and surface temperature and consequently on the machining performance. Supplying the cryogenic coolant is a technological challenge [4][8][9]: Since the cryogenic liquid inside the reservoir maintains on its liquid/gas saturation condition, any small heat transfer or pressure drop inside the coolant feeding system will evaporate a portion of the liquid with a combination of boiling and cavitation effects. The complexity of the cryogenic flow, as a saturated two-phase flow with phase changing, cavitation, and boiling effects in complex geometries, is a challenge for experimental studies. Despite the higher uncertainty and technical limitations of experimental investigations, numerical simulation could provide reliable results and calculate the temporal behavior of every variable at any place inside the domain.

Contrary to several studies in simulating the machining processes, the use of computational fluid dynamics in machining processes is very limited. Although there are some CFD analyses for machining applications, like [28][29][30], the studies on milling are limited to the work of Najiha and Rahman in which an initial analysis on MQL cooling [31] was carried out. In Tahri et al. [32], some CFD simulations of cryogenic coolant inside the simplified geometry of the milling tool were reported. No relevant research into the behavior of the cryogenic coolant inside the feeding

system and the effect of the working conditions and geometry on the performance of the cooling system has been found.

Despite numerous studies on cryogenic cooling, computational analysis of the coolant is rarely considered. Specifically, analysis of the cavitation and its role on the hydraulic efficiency of the coolant feeding system, the role of coolant pressure, and estimating the distribution of the coolant over the inserts and machining zone are the main novelty of this paper.

Moreover, a proper experimental verification procedure was conceived. Milling tests under different cooling conditions were carried out. The cutting forces measurements were interpreted exploiting a mechanistic model that helped understanding the role of the coolant on the main mechanisms involved in cutting. The analysis of the chip morphology supported and extended this analysis.

This paper tries to introduce some of the issues related to the cryogenic cooling in milling applications and provide computational simulations on the fluid mechanics aspects of the coolant flow, including hydraulic efficiency, cavitation, and jet impingement. For this purpose, several analyses on various parts of the system are conducted. Due to their characteristics, they were categorized as “internal flow” and “external flow” simulations.

In internal flow simulations, efforts focused on the incidence of hydrodynamic cavitation inside the tool channels. Because of that, a Homogeneous Equilibrium Model (HEM) was utilized to predict the formation, and distribution of the cavitation inside the geometry. The role of coolant pressure in nozzle flow efficiency was investigated afterwards. Then the coolant behavior inside the head channels was simulated and the importance of the cool-down process was emphasized by studying on the role of the milling head temperature on the phase and flow rate of the coolant. The simulation of the two-phase flow, including the phase changing and interaction of the phases in computational fluid dynamics, is a scientific challenge that affects several fields.

In external flow simulations, the analysis of the coolant distribution over the cutting inserts and machining area helps to improve the performance of the cooling system. For this purpose, a Volume of Fluid (VOF) solver is employed to predict the liquid interfaces with the solid and gas domain to predict the distribution of the coolant over the milling inserts, machining area, and surrounding air. Simulations focused on the distribution of the coolant jet flow in the air and then the interaction of the coolant jet in the cutting area. Results of these simulations (summarized in Figure 1) could provide a better understanding of the cryogenic coolant delivery for milling applications.

In cryogenic cooling, nucleate boiling is the most efficient boiling regime to consider for engineering problems [33]. For the quenching process, designers try to avoid critical heat flux which leads to a steady film boiling regime and the Leidenfrost effect [34] [33]. This phenomenon is common in boiling processes with natural convection of the coolant or immerged systems [35][36]. In the current setup, due to the high velocity of the coolant and the forced convection [35][37], local boiling films will be washed away rapidly with the coolant jet and cannot form a steady vapor film around the hot spots. An analysis of the conjugate heat transfer in the cutting region, mostly by evaporation of the cryogenic coolant over the surface, requires extensive studies

with detailed information about the heat flux in the solid parts and the coolant distribution over the surface. The results of this paper provide proper information about the distribution of the coolant in the cutting area, which could be coupled with a FEM analysis in the future to provide a reliable heat transfer analysis.

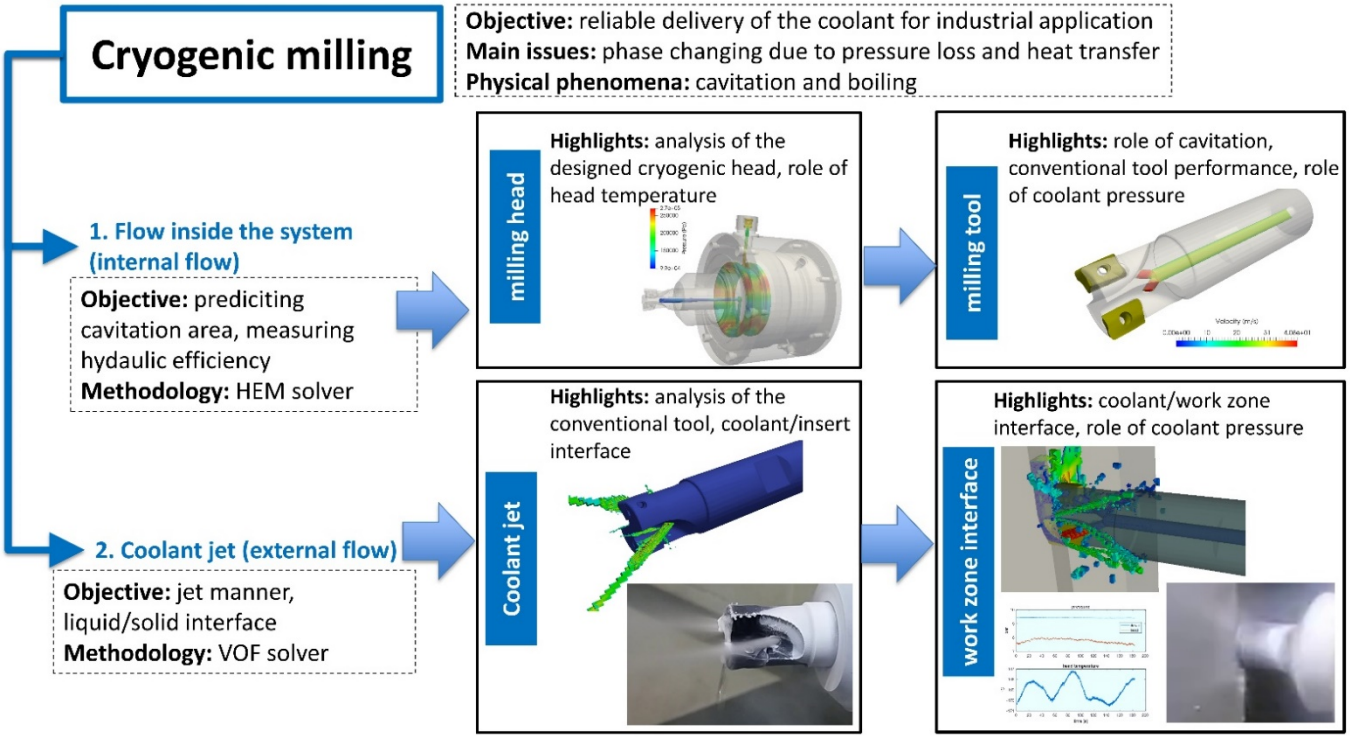

Figure 1: Schematization of the performed analysis.

The paper is structured as follows. Section 2 introduces issues and challenges connected to the cryogenic coolant feeding in machining applications. In section 3, the experimental setup and industrial plant is presented. Afterwards, the theory and details regarding the HEM solver for simulating the cavitation and two-phase flow are illustrated in section 4. Then, in the analysis section, the description of the simulations and their results is presented in detail, for internal flow (section 5) and external flow simulations (section 6). In section 7, the experimental verification session is described, and the results are critically discussed. Conclusions are reported at the end of the paper.

2. Challenges in utilizing cryogenic cooling for machining applications

Two physical problems during cryogenic fluid transfer have wide-ranging impacts on the overall system design: heat leak in cryogenic transfer and pressure drop during transfer of fluids. The transfer piping design should accommodate the desired heat transfer requirements as well as the fluid transfer conditions necessary to accommodate the overall system design. Some specific design considerations for cryogenic transfer lines are optimization of the heat leak and control the cavitation and two-phase flow inside the feeding line and channels.

When the cryogenic liquid flows into the typical transfer line which is initially at room temperature, at first, all the liquid which enters the pipes is quickly evaporated, and nearly all the line will contain only gas. As the process continues, a length of the upstream end of the line will be cooled to the saturation temperature, and this portion will contain the pure liquid phase. Downstream of the section, there will be a region in which both liquid and vapor exist, and in the remaining part of the line, only gas will be flowing. As the line is further cooled by liquid evaporation, the liquid phase will persist farther along the line until finally liquid will be discharged at the exit [38].

Heat flow into a pipe carrying a liquid cryogenic has two objectionable consequences: First, it wastes liquid by causing evaporation, and second, the formed vapor reduces the carrying capacity of the line. Two-phase flow has been studied by many researchers and is extremely complex [39][40][41]. For cryogenic fluids, the complexities of ordinary two-phase flow are further compounded because of huge heat transfer caused by temperature gradient and continuous phase changing between liquid and vapor in a saturated flow caused by cavitation and boiling [39][40].

There are three diverse kinds of two-phase flow in a cryogenic flow transfer line: 1. a homogeneous mixture of vapor bubbles in the liquid; 2. “slug” flow consisting of alternate regions of pure liquid and pure vapor, each filling the pipe; and 3. annular flow, where the liquid flows along the annular region next to the wall [39]. Figure 2 shows these two-phase regimes inside the pipe during the cool-down process.

In addition, even if the wall is cooled down and the heat leak is negligible, at positions where the pressure falls below the saturation pressure, cavitation occurs and forms the attached or detached vapor clouds inside the feeding system.

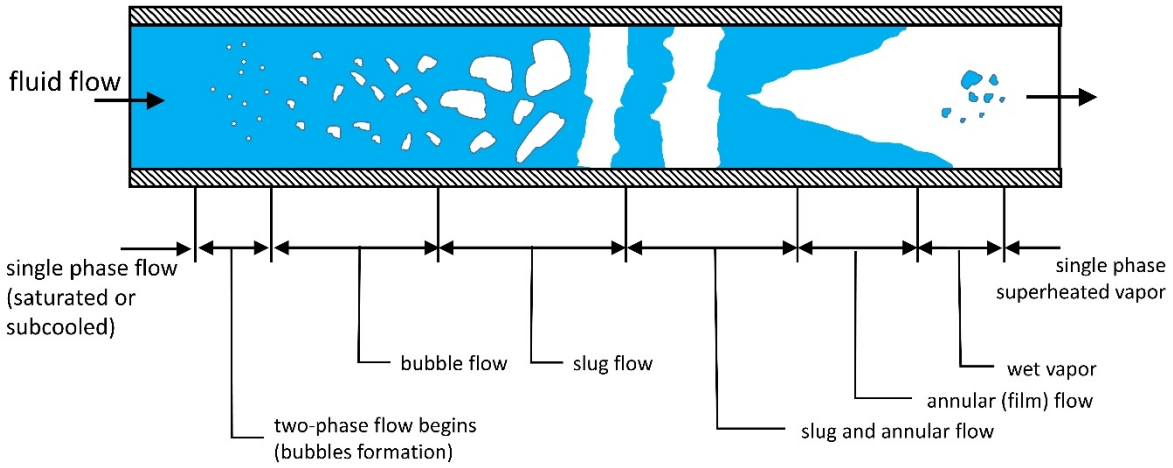

Figure 2 Schematics of two-phase flow regimes inside a pipe during the cool-down process, based on [39][40]

Proper design of the coolant feeding line is a vital element in cryogenic cooling. According to the performance of the feeding line, flow delivery after the cool-down transient stage could show three

regimes of delivery: zero delivery, fluctuating delivery, and continuous delivery. Pusavec et al. [27] detected these three regimes with their phase sensor during their experiments.

The complexity of the two-phase flow and its dependency to the working conditions persuade designers to avoid two-phase flow. But sometimes two-phase flow is unavoidable. It must be noticed that even if the feeding line is well designed, it is not an ideal design with zero heat transfer and zero pressure loss. Moreover, achieving the ideal 100% liquid ratio at the outlet is not realistic, as the cryogenic liquid at reservoir stays in its saturation state, and any minimal heat transfer and pressure drop will evaporate a portion of the flow.

Generally, the design of the cryogenic feeding line is a trade-off between cost and required performance. If the price of the coolant is relatively small, it could be profitable to provide occasional gas-liquid separators along the transfer line and allow most of the vapor formed in the line to escape continuously at these places during transfer [38].

3. Description of the plant and experimental setup

The experimental setup, taken as a reference for this research, is equipped with a LN_2 feeding system. In Figure 3, the schematics of this feeding system are presented. Liquid nitrogen is stored inside a tank, called Dewar. Vacuum jacketed flexible pipes are selected for transferring the coolant to the machine. As suggested before, a liquid-gas separator purges the evaporated nitrogen in the transfer pipes to reduce the cool-down time and fluctuating delivery of the liquid at the feedline end. Despite using the vacuum insulated flexible pipes with very low heat leakage and using this gas separator close to the milling head, the heat transfer and pressure drop after the gas separator inside the electro valve, spindle, and joints are the remaining issues, due to the limits of the technology.

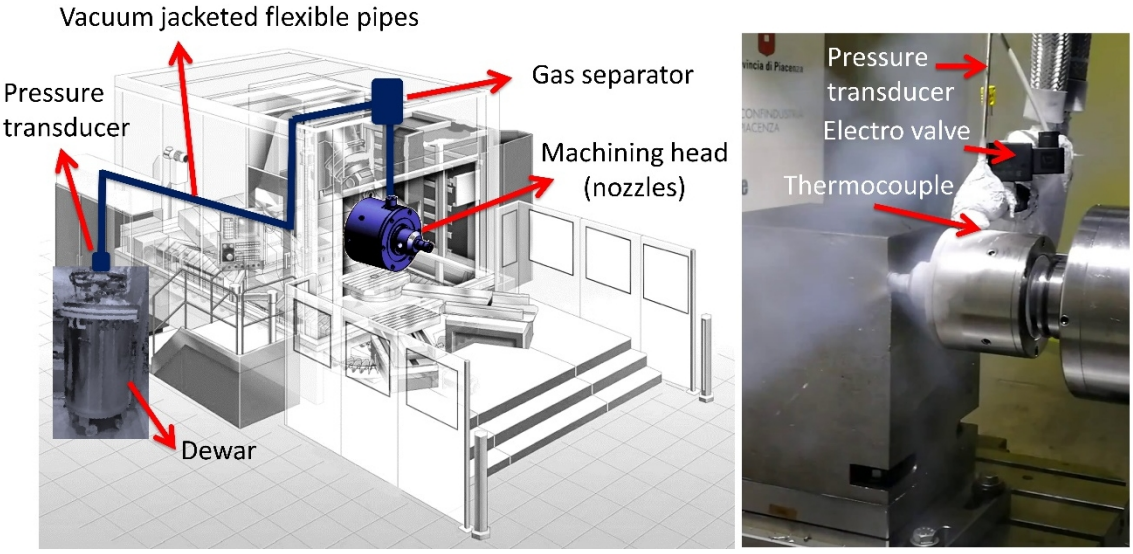

Figure 3 Schematics of the plant and cryogenic coolant feeding system; details of the cryogenic head, pressure and temperature measurements

For this study, a milling cutter, from SANDVIK Coromant products, "R390-020B20-11L CoroMill® 390 square shoulder milling cutter" with Z = 2 inserts and diameter of D = 20mm was selected.

So far, few industrially compatible cryogenic coolants delivery solutions have been developed for milling applications. Some of them are even patented, i.e. Rozzi et al. [42], [43]. For this reason, a specific cryogenic head was designed, in collaboration with an industrial partner (Jobs SpA- FFT group), exclusively for this application. The cryogenic fluid feeding to the tool nozzles is ensured by a rotating collector scheme. Materials and bearings suitable for cryogenic applications were selected. More specifically, an insulation system was conceived in order to protect the sensitive parts of the machine from low temperature issues. Even the milling cutter was modified in order to improve the insulation properties. A specific gas separator system was adequately designed and optimized to efficiently purge the evaporated nitrogen from the feed line. Moreover, a proper ventilation system was also developed to remove the nitrogen gas from the plant and reduce the risk of a lack of oxygen for operators.

The schematics of the milling cutter and cryogenic head are shown in Figure 4.

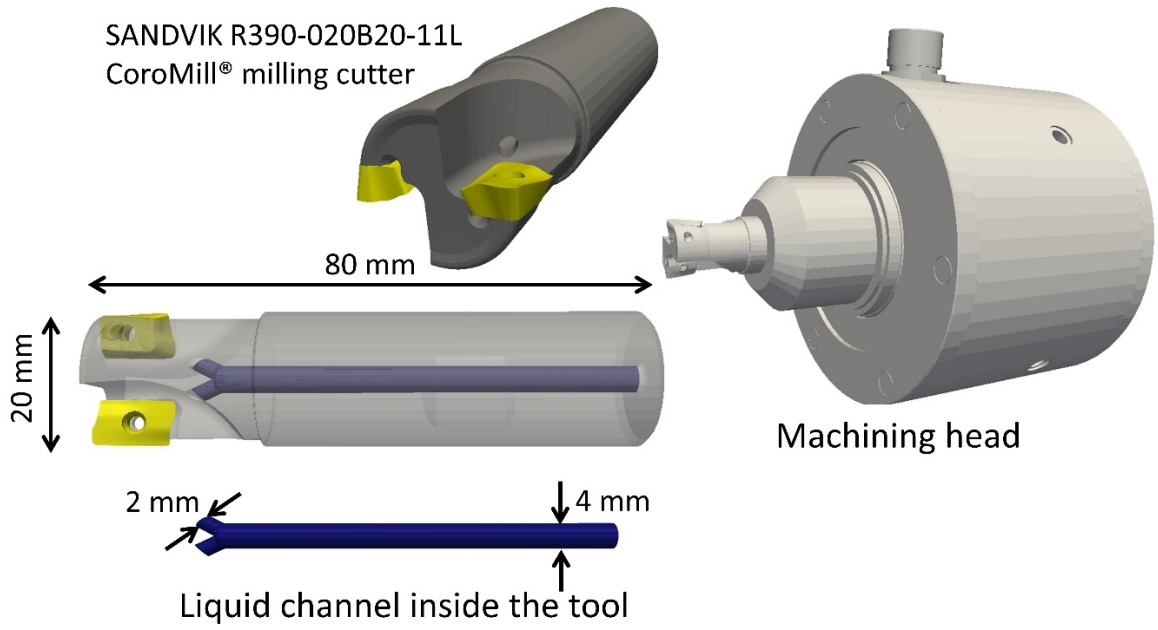

Figure 4 Schematics of cryogenic head, milling tools, and inserts

Initial experimental studies were applied to understand the behavior of the coolant feeding system. In these tests, experiments with coolant pressures, varying from 1 to 8 bar, were carried out. Coolant mass flow rate is measured by continuously weighting the tank during the tests. The milling head wall temperature is measured by installing thermocouples close to the wall. Tank and line pressure are measured during the tests. Figure 5 shows the adopted milling head in different states during the tests. These experiments were used to improve the simulation assumptions, evaluate the accuracy of the results, and consolidate the conclusion from the simulation results. Proper experimental cutting tests were carried out to verify the numerical findings in section 7.

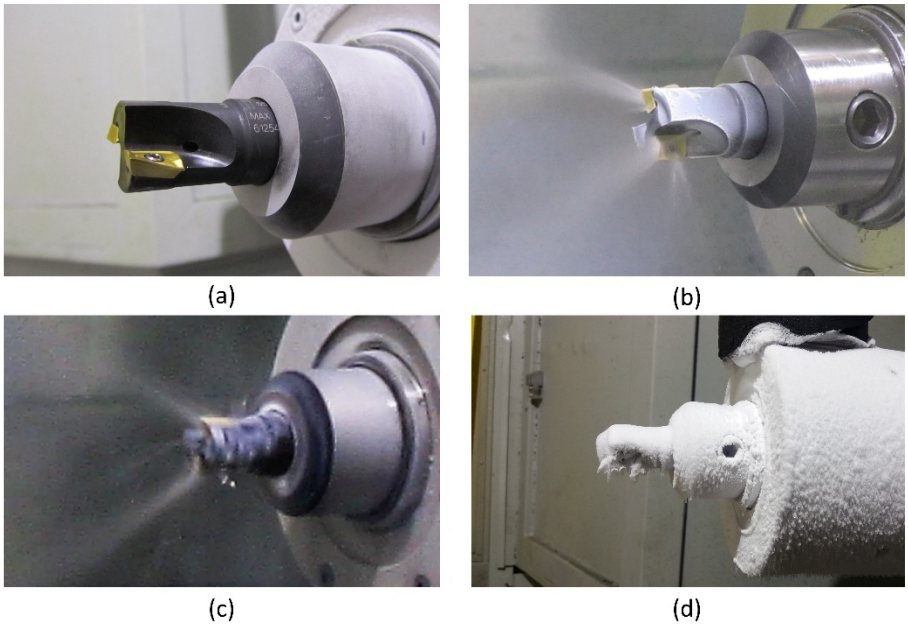

Figure 5 Captured images during experimental tests: (a) shows the tool during the cool-down stage, (b) shows the tool during the steady flow stage, (c) relates to the steady phase when the milling head is rotating, and (d) relates to the end of the test, when coolant flow is turned off, and surfaces are covered by a frozen water from the atmospheric humidity.

4. Theory of the two-phase flow and simulation solver

In continuum mechanics, the equations describing the conservation laws of mass, momentum, and energy are well established. Appropriate constitutive equations then complement these field equations like thermodynamic state, energy transfer, and chemical reaction. These constitutive equations specify the thermodynamic, transport and chemical properties of a constituent material. It is to be expected that the conceptual models for multi-phase flow should also be formulated regarding the appropriate field and constitutive relation. However, the derivation of such equations for multi-phase flow is considerably more complicated than for single-phase flow.

4.1. Hydrodynamic cavitation

Even with assumption of adiabatic condition inside the cryogenic coolant feed line (assuming the line is cooled down and the insulation is ideal and without any heat transfer), or that the cryogenic liquid is subcooled enough to compensate the system's heat leakage, hydrodynamic cavitation inside the system could occur because of the local pressure decrease. Hydrodynamic cavitation is the formation of bubbles and cavities in a liquid, due to the decrease in static pressure below the vapor pressure, caused by the geometry through which the fluid flows. Figure 6 shows the difference between boiling and hydrodynamic cavitation. In the case of boiling, the temperature is increased at a constant pressure, while for hydrodynamic cavitation, the temperature is not altered, and the pressure decreases.

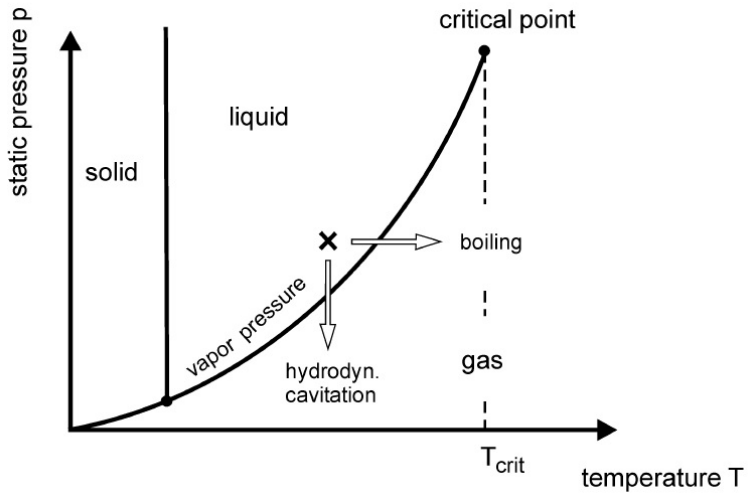

Figure 6 Description of the cavitation and boiling in a pressure-temperature diagram [44]

When the liquid enters to an area with a reduced cross section, or sudden rotation in the solid wall direction, the flow will accelerate to satisfy the conservation law. Assuming a simplified one-dimensional, stationary, frictionless, incompressible, and isothermal flow, the Bernoulli equation as

$$P_1 + \frac{\rho {u_1}^2}{2} = P_2 + \frac{\rho {u_2}^2}{2}, \tag{1}$$

can be used to explain the fact that an increase in flow velocity (u) from point 1 to point 2 further downstream leads to a decrease in static pressure (p). The lowest static pressure is reached at the edges in the recirculation zones of the so-called vena contracta. The cavitation zones develop along the walls, can separate from the walls, disintegrate finally into bubble clusters, and may begin to collapse inside the channel. Also, they could attach to the wall and reduce the effective cross section of the flow. This artificial resistance will reduce the flow rate and capacity of the feeding line. The role of channel geometry is significant concerning the development of cavitation. The more the edges are rounded, the smaller the flow contraction and the smoother the decrease of static pressure. To characterize the flow capacity of a flow path geometry, the "discharge coefficient" is usually defined as:

$$C_d = \frac{\dot{m}}{A_0\sqrt{2\,\rho\,dp}} \tag{2}$$

which is the ratio between the actual mass flow rate ($\dot{m}$) and theoretical mass flow rate from the Bernoulli equation ($A_0\sqrt{2\rho dp}$). In this phrase, A_0 refers to the minimum cross section of the channel, ρ is the density of the incompressible flow, and dp is the pressure difference between the inlet and outlet sector. The discharge coefficient is a value between 0 and 1[45][46].

4.2. Description of the simulation methodology

As discussed above, analysis of the feeding system of the cryogenic coolant is a sophisticated problem with several issues. Each part of the system has its specific geometry and working

condition and several physical phenomena are coupled together. Finding a comprehensive method which could consider all these issues with their microscopic and macroscopic characteristics is still unsolved. But focusing on each part and analyzing the issues could increase the knowledge about it and help us to improve the design and development of a reliable and applicable cooling technology.

In this study, it was tried to analyze the flow conditions inside the cooling channels, specifically inside the milling head and milling tool to evaluate their flow delivery efficiency. Due to the importance of the cavitation in these parts, a homogeneous equilibrium model (HEM) is used to predict the cavitation and its growth inside the milling tool. This method is widely used in different studies for different applications, e.g. [47][48][49][50][51]. Liquid and vapor phases are assumed to be mixed perfectly in each cell while also considering the compressibility of both phases. Likewise, pressure and density are related to each other with a barotropic equation of state. Details about the theory of this method could be found in [47][48][49]. After that, behavior of the coolant jet and its interaction with milling inserts, the machining area and surrounding air are analyzed. For this purpose, a Volume of Fluid (VOF) model was selected due to its ability to capture the flow interfaces. Details about this model could be found in [49][52] [53].

The governing equations are solved using finite volume Computational Fluid Dynamics (CFD) methods presented in the OpenFOAM technology. OpenFOAM (Open Source Field Operation and Manipulation) is a C++ toolbox for the development of customized numerical solvers with pre- and post-processing utilities for the solution of continuum mechanics problems [54].

Due to the presence of solid boundaries and small dimensions, the flow behavior and turbulence structure are different from free turbulent flows. This implies that the inertia forces are greater than the viscous forces at these scales (large Reynolds number). Due to the performance of the $k\omega$-SST turbulence model and its benefits for simulating internal flows with high Reynolds number and adverse pressure regimes [55], this model was selected for the internal flow studies in the current work. For external flows, the $k-\varepsilon$ model was selected due to its robust characteristics in free streams.

Running the simulation, physical parameters inside the domain are updated in each time step until reaching the final state. The Courant number and the acoustic Courant number are controlled to prevent divergence. To define the proper limiting condition for the end of the simulation, mass conversion is checked by testing the inlet and outlet mass flow rates from two aspects: first, due to the difference of the mass flow rate between the inlet and outlet sectors, and second, the change of the values in comparison to the previous time step [47]. As an example, Figure 7 presents the results for the mass flow rate in the inlet and outlet sectors of a simulation for internal flow simulation with P = 8 bar.

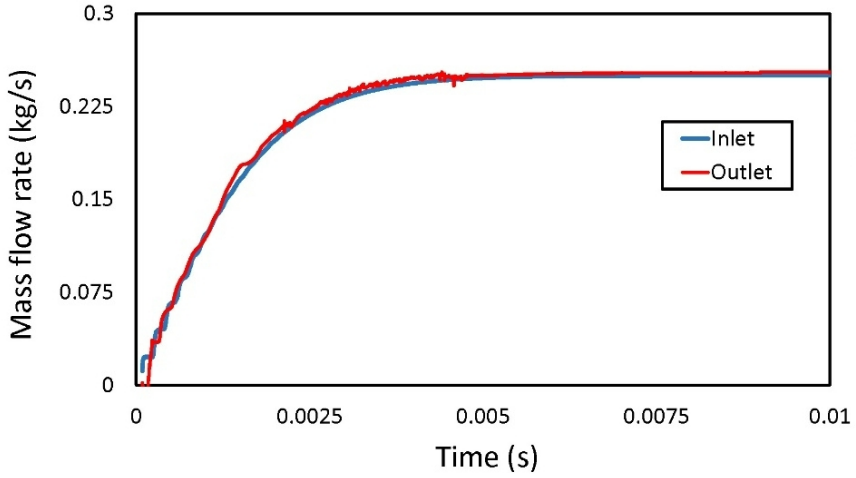

Figure 7 Comparison of the results for the mass flow rate in the inlet and outlet sectors of the milling tool with 8 bar inlet pressure

5. Analysis of the internal flow

5.1. Simulations of the flow inside the milling tool

As mentioned before, the role of the flow channel's geometry and working condition on the formation and distribution of the cavitation inside the feeding system and consequently the efficiency of the flow delivery is highly important. As discussed earlier, the likelihood of cavitation forming inside the milling tool is high. The geometry of the milling tool is selected from the commercial products for conventional cooling. To focus on the role of the tool channels on the formation of the cavitation and phase changing inside the tool, it is assumed that the liquid nitrogen is entering to the milling tool as a 100% saturated liquid, even if this assumption is idealistic and far from the reality of the experimental investigation. In Figure *8*, details about the geometry of the flow channel are presented. As shown here, coolant flow inside the tool divides in a Y-shaped branch, and each side injects the jet over a milling insert.

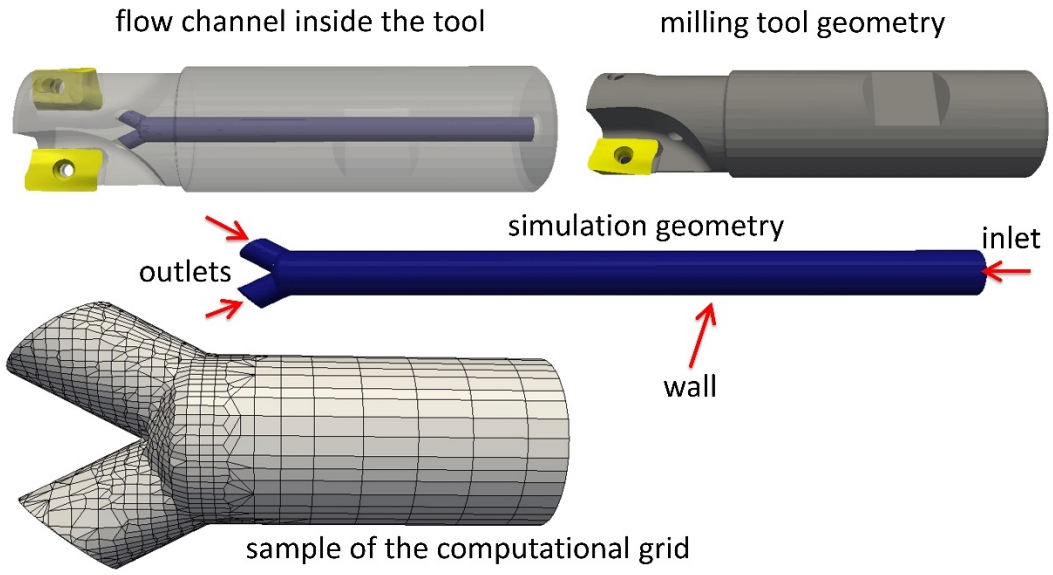

Figure 8 Geometry of the milling tool, its internal geometry, simulation geometry, and sample of the computational grid

For the boundary conditions, the pressure at the nozzle inlet is set at 2, 4, 6 and 8 bar. It was decided to investigate such a range of pressure because of the feasible range of the experimental setup, as pressure values above this range are not supported with current commercial liquid nitrogen tanks and flexible pipes.

At the nozzle outlet, atmospheric conditions are assumed. A no-slip condition is assumed for the walls, and saturation properties for liquid nitrogen are read from NIST tables [56]. Simulation parameters, boundary conditions, non-dimensional wall distance (y+), and grid properties of these internal flow simulations and further studies in sections 6.1 and 6.2 are presented in Table 1.

Table 1 CFD simulation setup and grid properties for internal and external flow simulations (P = 8 bar)

	Internal flow (section 5.1)	External flow (section 6.1)	External flow (section 6.2)
Two-phase model	HEM	VOF	VOF
No. of cells	~65,000	~350,000	~2,000,000
Grid cell type	Hexahedral, polyhedral, and prisms	Hexahedral, polyhedral, and prisms	Hexahedral, polyhedral, and prisms
y +	0.79	1.21	0.85
Reynolds number at the throat	526,000	526,000	526,000
Turbulence model	kω − SST	kε	kε
Wall function	No-slip velocity, kω wall functions	No-slip velocity, kε wall functions	No-slip velocity, kε wall functions
Min. cell volume	1.47e-13	4.8e-12	7.03e-13
Max. cell volume	8.7e-10	5.4e-9	1.07e-9

In Figure 9, the distribution of the flow velocity and pressure is presented for a cut plane, close to the branch and injector's end. As presented in the above row, by increasing the coolant pressure, the velocity of the coolant increases, and consequently, local vorticities increase after the divergence in the geometry in the channel branch. The lower row of the Figure 9 shows that the pressure of the coolant in studies with higher inlet pressure is high but when approaching to the nozzle end, the pressure is reduced significantly to update its condition with the outlet atmospheric condition.

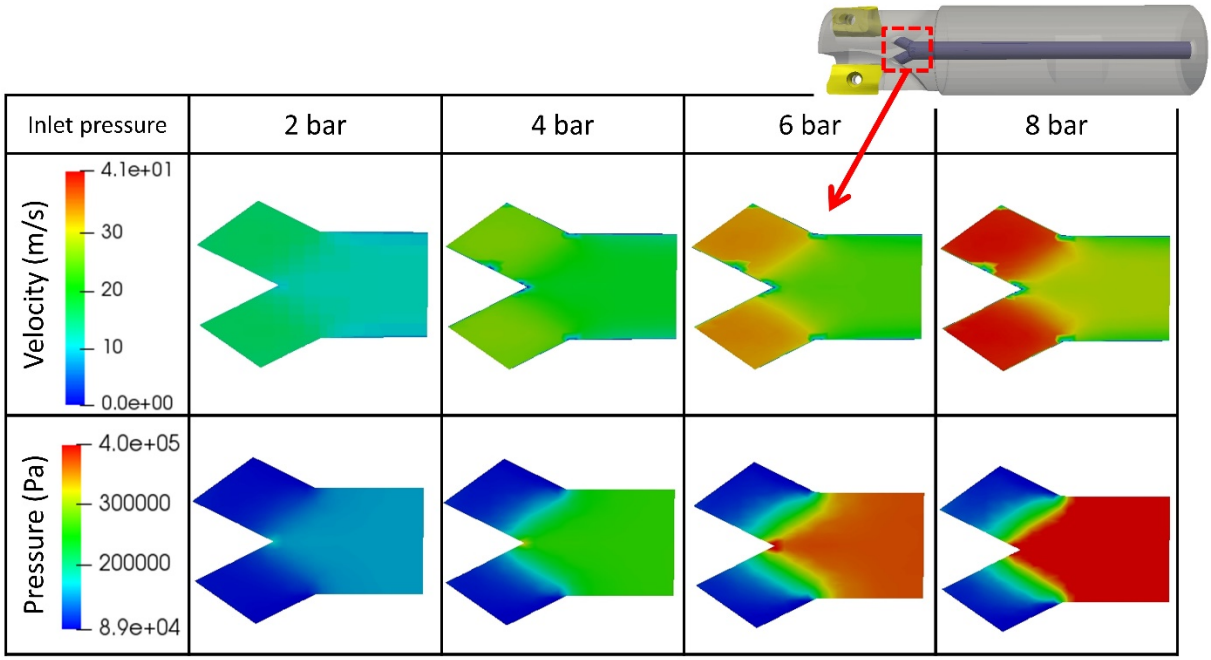

Figure 9 Distribution of the flow velocity and pressure in a cross-section close to the outlet. Results for simulations with different coolant pressures are compared.

Figure 10 shows the cavitation area close to the nozzle end for simulations with two assumptions of 2 and 8 bar inlet pressure. When the pressure drops below than the saturation pressure of the liquid at that temperature, the flow evaporates, and cavitation starts. As presented in Figure 10 in the study with 8 bar inlet pressure, the cavitation area is larger than in the study with lower pressure. In fact, the role of higher velocity close to the solid wall and a sharp change in the area section leads to increased vorticities and consequently a reduction of the local pressure.

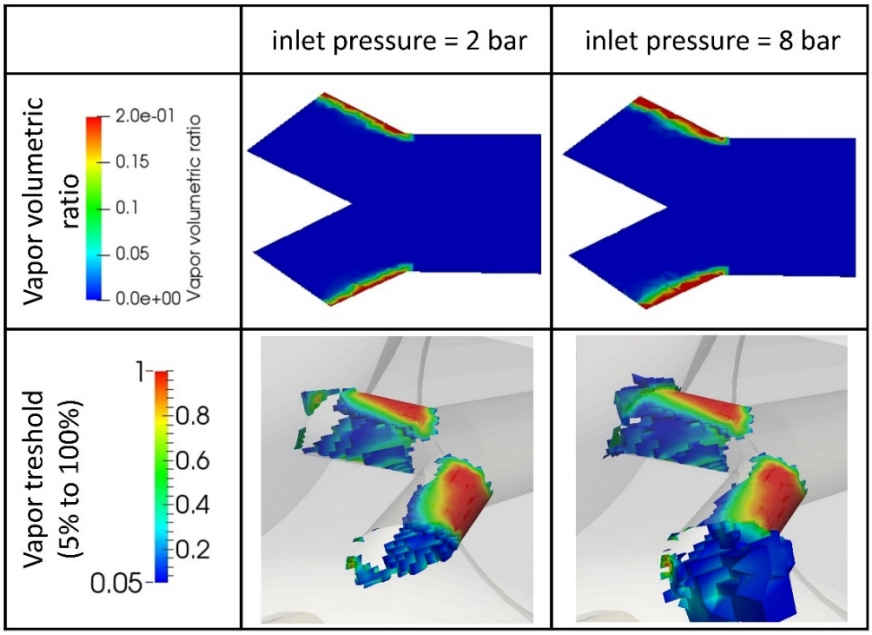

Figure 10 Comparison of the cavitation regime for P coolant equals to 2 and 8 bar: the threshold of the cells with minimum 5% vapor close to the injector outlet, colored by vapor volumetric ratio

In Figure 11, a virtual probe is defined to measure the results for flow properties across this line. This line is defined in the middle of the flow of one of the channels, starting from the branch area and ending at the nozzle outlet. As presented in the pressure graph, despite the higher value of the pressure in the study with 8 bar inlet pressure, the pressure value reaches the 1 bar pressure after the branch. The density of the flow in each cell is calculated according to the percentage of the liquid and vapor in that cell. As illustrated in the density graph of Figure 11, for the study with 8 bar inlet pressure, density is reduced in a larger length of the probe, and the value of the mixture density is lower in that area. This probe helps to better quantify the distribution of the cavitation and two-phase flow inside the nozzle. This cavitation area and the presence of a two-phase mixture works like a resistance and virtually reduces the liquid cross section.

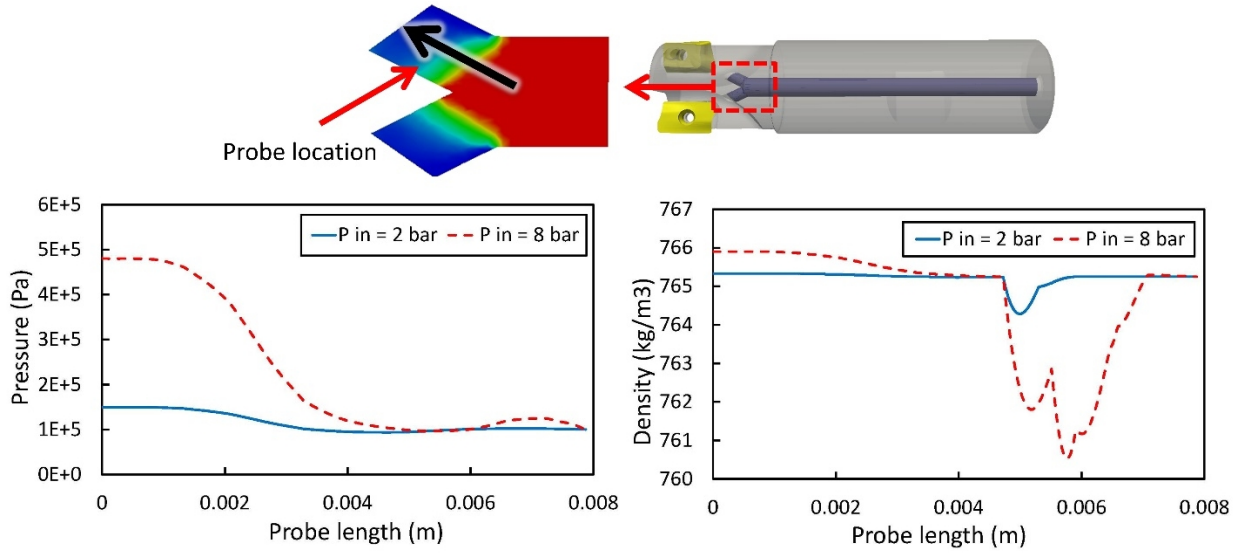

Figure 11 Distribution of pressure and density over a line at the middle stream of the nozzle hole channel: comparison of two different pressure setups

In Figure 12, the results for the coolant flow rate and nozzle discharge factor are presented. As shown in the mass flow rate graph, the mass flow rate is increased by raising the inlet pressure. But as presented in the discharge factor, which compares the flow rate from the simulation and the theoretical flow rate from equation (2), the discharge factor of the nozzle is reduced when the pressure is raised. The increment of the cavitation region in the studies with higher pressure is the reason for this loss in nozzle efficiency. To better understand the role of cavitation, another simulation has performed with 6 bar inlet pressure, and intentionally turned off the cavitation module of the solver. As presented in the discharge factor graph, the red column shows the result without considering the cavitation and highlights the role of cavitation on the efficiency of the coolant feeding system.

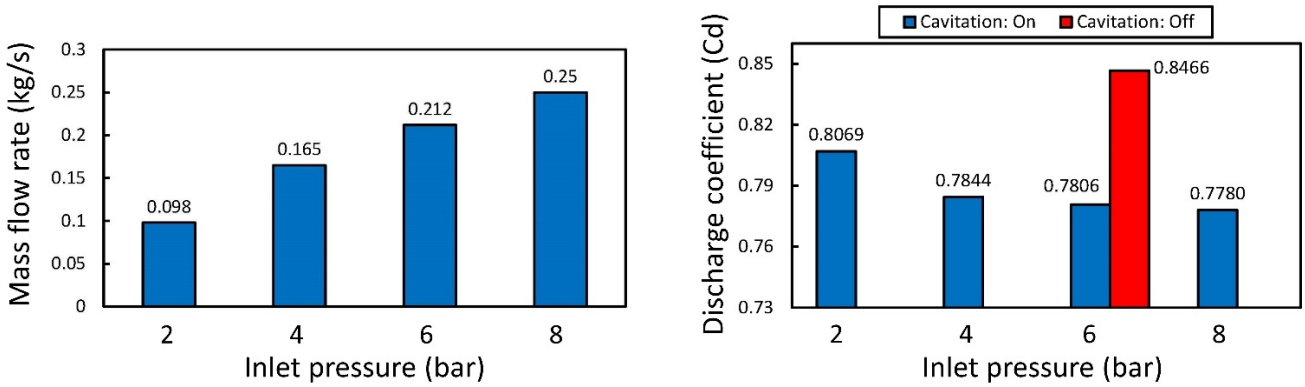

Figure 12 Results for the coolant mass flow rate and nozzle discharge factor for analyzing the flow inside the milling tool

The results of these simulations show that the discharge factor of the milling tool decreased by raising the coolant pressure. Therefore, as the flow rate is proportional to the squared pressure,

using high pressure coolant would waste the coolant without any reasonable improvement in cooling conditions. In real application (like the one reported in Figure 3), a pressure range from 1bar to 3 bar would be suggested. This means that the Dewar pressure set-point needs to be tuned to low-pressure range.

In addition, in a low-pressure setup, the discharge factor of this conventional tool, even while considering cavitation inside the channels, is about 80% which is in the range of commercial injectors. As a conclusion, the hydraulic performance of this commercial tool is acceptable for cryogenic application, especially with a low-pressure coolant.

5.2. Simulation of the flow inside the milling head

For this part of the study, it is tried to simulate the coolant flow inside the special milling head, designed and developed by an industrial partner for cryogenic milling. This head has a feeding ring which aims to feed the coolant to the milling tool during the work and rotation of the head. In Figure 13, the geometry of the simulation is presented in the transparent schematics of the milling head and milling tool. As presented in Figure 13, the dimensions of this ring are relatively larger than the milling tool, and consequently, the flow velocity is low inside this ring. For this reason, in simulation of the flow inside the milling head, cavitation formation was insignificant. However, the milling head and milling tool, are the only non-insulated parts of the coolant feeding system, made from steel, with relatively heavy mass and large external dimensions and technical difficulties for an effective insulation. Therefore, heat transfer and boiling inside these devices is most probable and not ignorable. For this study, results of low-pressure experimental measurements which are presented in section 7, show 2.4 bar pressure before the milling head. For the simulation setup, it is assumed that nitrogen enters to the head as 100% liquid. Also, role of the rotation is neglected, and it is assumed that the feeding system is fixed at a position like Figure 13, left side. Results of the flow pressure inside the coolant passage are presented in this figure. Simulation results show that, with assuming 100% liquid at the entrance, the mass flow rate would be $101\ \mathrm{kg/h}$ while the experimental measurements with 2.4 bar pressure was $65 \pm 5\ \mathrm{kg/h}$. The difference between simulation and experimental measurement could have several reasons. Other than the measurement techniques and experimental setup, the physical properties of the nitrogen when entering the milling head are very important. As shown in the preceding section, a cavitating area inside the nozzle could reduce the discharge factor from 84.6% to 78.0% (Figure 12), so if nitrogen entered to the head with some cavitation and bubbling produced before the milling head, the hydraulic resistance of the line would be higher and accordingly, the actual flow rate would be lower than the current simulation.

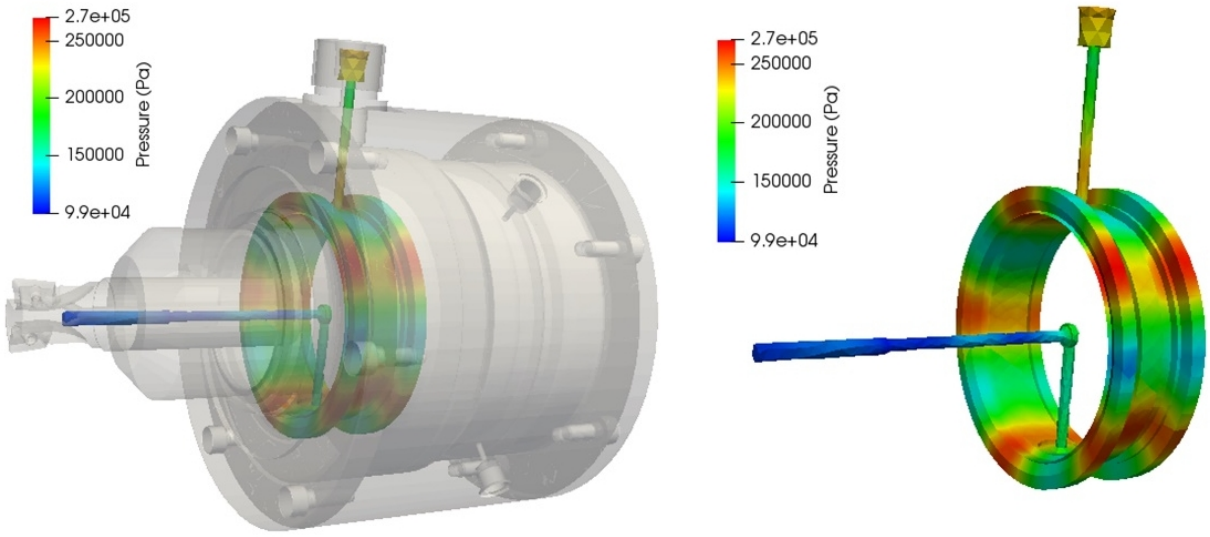

Figure 13 Results for the simulation of the flow inside the spindle coolant passage

Previous analysis shows that the assumption of full liquid nitrogen entering the head is not realistic, and the experiments show that the actual flow rate is lower than the results with this assumption. A revision in design of the feeding system, would be resulted to higher percentage of the liquid entering to the machine and higher cooling capacity.

To estimate the role of heat transfer inside the head and the importance of the cool-down process, in this step, two analyses have been performed with different assumptions. For the first analysis, it is assumed that the head is at room temperature and the flow passage walls are at 300 K constant temperature. For the second analysis, it is assumed that the head is cooled down and the flow passage walls are at 100 K, selected from the experimental measurements. Liquid nitrogen at 95 K enters to the flow passage; there is no phase changing, and the transferred heat is used to heat the liquid with convection phenomena. With these assumptions, the temperature of the liquid at the nozzle outlet is calculated with the assumption of this heat transfer is spent on the evaporation of the liquid nitrogen by assuming the following calculation:

$$\dot{m}_{tot}\, C_p \Delta T = \dot{m}_{evap}\, h_{evap} \Rightarrow \frac{\dot{m}_{evap}}{\dot{m}_{tot}} = \frac{C_p \Delta T}{h_{evap}} \tag{3}$$

Equation 14 is used to process the simulation results which are presented in Table 2.

Table 2 Analysis of the role of head temperature on coolant phase changing

No.	Milling head temperature	Flow temperature at inlet	Flow temperature at outlet	Equivalent $\frac{\dot{m}_{evap}}{\dot{m}_{tot}}$
1	300 K	95 K	179 K	100%
2	100 K	95 K	97.5 K	1.7%

As in this table, if the head flow passage walls are cooled down until 5 K above the coolant temperature, a small portion of the liquid (1.7%) will evaporate inside the head because of the heat loss. But if the head is not cooled down and flow passage walls are at room temperature, all the liquid will evaporate inside the flow passage. Hence, a better understanding of the zero-delivery discussed earlier and its projection in Figure 5, part (a) have been presented.

6. Simulation of external flow

After analysis of the coolant behavior inside the cooling channels, this section of the paper, focused on the coolant jet behavior. First, some efforts implemented to simulate the coolant jet over the milling inserts and inject it into the atmosphere, then the interaction of the coolant jet with the cutting area was simulated. Simulation of the coolant jet and its interaction with the milling inserts and cutting area helps to evaluate the performance of the cooling system and possibly improve the design and working conditions. These results could be employed for future studies, by adjoint simulation of cutting and conjugate heat transfer between the solid and fluid substances to demonstrate a comprehensive analysis of the cryogenic milling. Due to the importance of a reliable prediction of a liquid interface with inserts, cutting area, and surrounding air, CFD simulations were conducted by using a VOF model from the OpenFOAM package with its proven performance for these objectives [40, 45].

6.1. Simulation of the coolant jet

To simulate the coolant jet over the cutting inserts, it was assumed that the flow is in its steady condition, the coolant line is cooled down, the milling tool is not rotating, and the jet after impinging to the milling inserts will be ejected into the surrounding air. These assumptions help to reduce the complexity of the process because of the rotating effects and permit experimental observations. Figure 5, parts (b) and (c) show the difference of the observations in non-rotating and rotating conditions. The computational geometry includes the internal channel of the milling head and a volume around the head is presented in Figure 14. Like previous studies, several simulations have performed with various coolant pressures ranging from 2 to 10 bar to understand the role of coolant pressure on the cooling jet. In Figure 14, the distribution of the velocity over a plane, tangential to the milling insert, shows the orientation of the jet close to the insert. The concentration of the liquid coolant in the cutting region, is in accordance with its design criteria for cooling the cutting region. However, the role of tool rotation is not considered in this simulation. Moreover, in the right side, the threshold of the liquid phase shows the behavior of the emerging jet in the area close to the tool. This result could compare with the experimental observations presented in Figure 5, part (b).

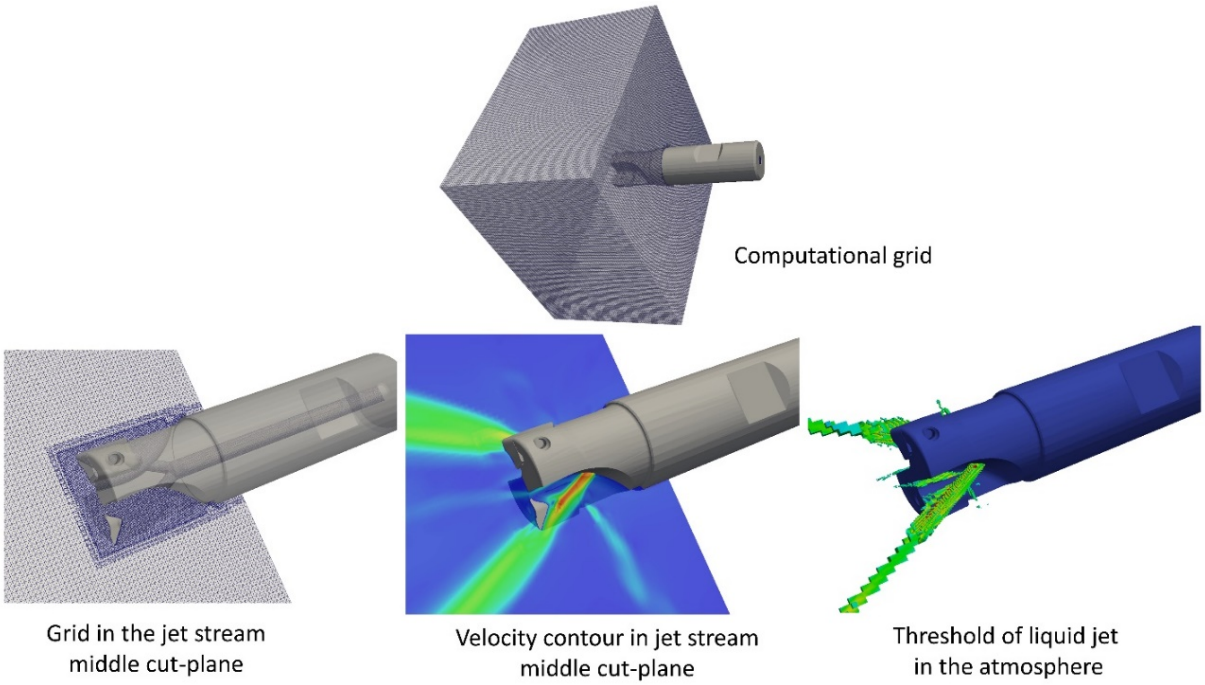

Figure 14 Steps for simulating of the coolant liquid jet in the surrounding air

Figure 15 shows the comparison of the coolant jet velocity in various inlet pressure setups. By increasing the coolant pressure, a high-speed jet impinges to the working surface which could offer both advantages and disadvantages for the cooling process.

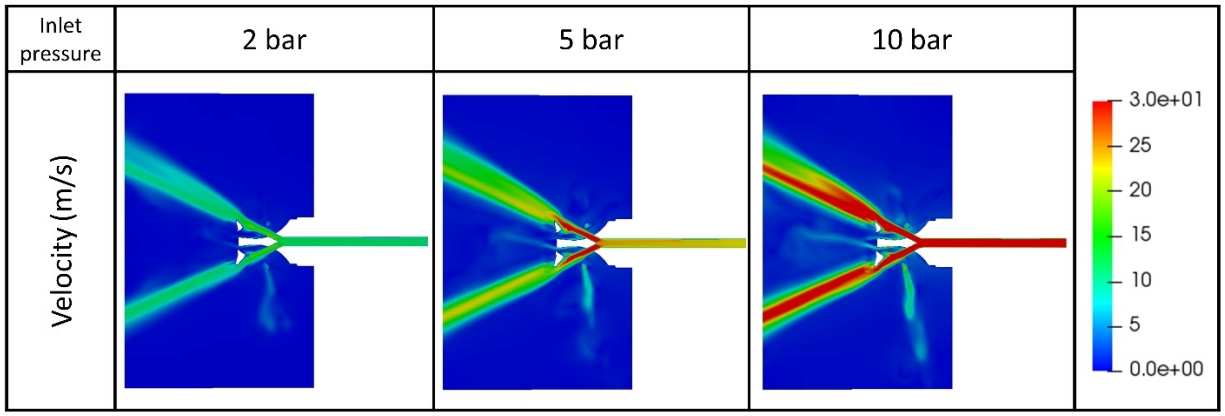

Figure 15 Distribution of the coolant velocity in a middle plane near the nozzle; comparison of the simulations with different coolant pressure values

The distribution of the coolant jet with cutting inserts is a noteworthy information for the cooling process. For that reason, it has tried to compare the distribution of the coolant over the milling inserts as presented in Figure 16. The upper row shows the distribution of the liquid jet over the surface, colored by the velocity contour, while lower row is colored by the liquid ratio contour. The role of the jet velocity is emphasized in these results. In higher coolant pressure, the velocity of the jet over the surface is specifically higher, but on the other hand, the higher velocity caused

the jet to reflect from the surface which is shown as a hollow area inside the liquid threshold. Moreover, when the jet has a high velocity, the liquid is rapidly washed from the surface which could be not efficient for surface cooling if the coolant evaporation time scales are not small enough to capture the inserts' heat. These investigations are in accordance to the findings from the internal flow simulations about advantages of using the lower pressure coolant.

Furthermore, Figure 16 shows that the orientation of the liquid jet is focused on the lower part of the insert, which is involved in milling operations with low axial depths of cut. It is worth noting that the jet is not facing to the flank of the insert (cutting edge) which is involved in milling operations with high axial depths of cut or in contouring millings. Future studies, by considering the rotation effects, coolant evaporation, and heat transfer inside the inserts could provide a better investigation into these issues to design and develop the optimal cryogenic cooling.

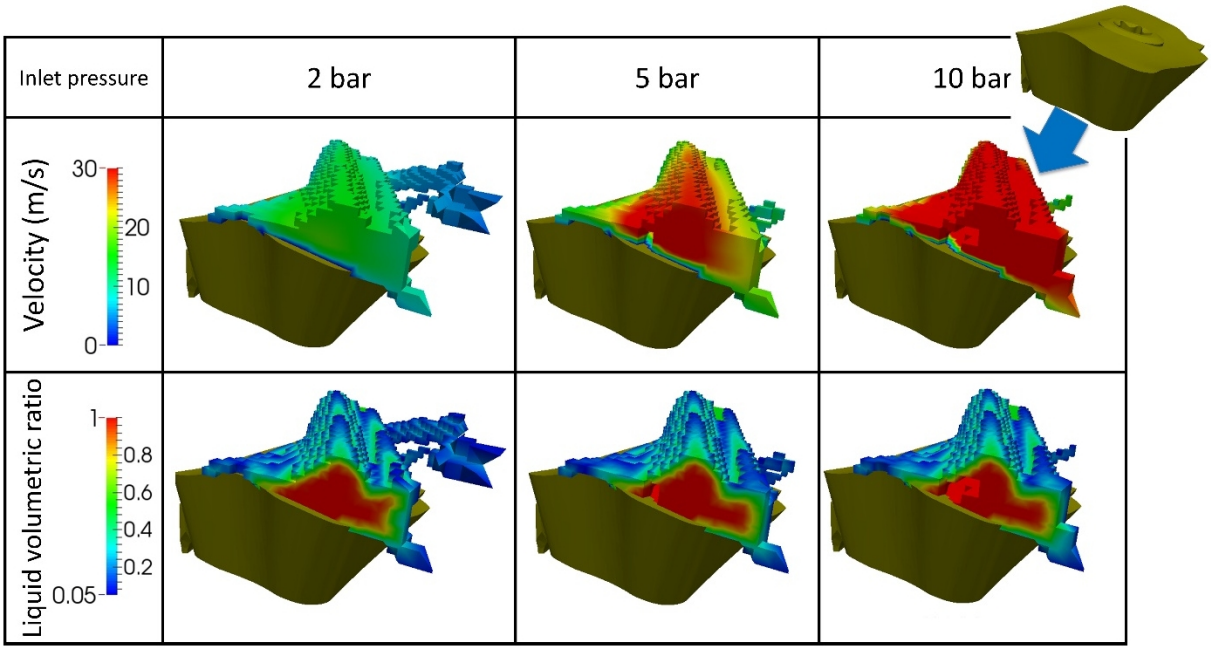

Figure 16 Distribution of the liquid coolant flow over the cutting tool (threshold of 5% to 100% liquid). The upper level shows the distribution of velocity while the lower row shows the distribution of the liquid ratio in the coolant

6.2. Simulation of the interaction of the coolant jet and the working area

In the last but not the least part of the analysis, the distribution of the liquid coolant in the working area is investigated in this section. To reduce the complexity of the simulation, the rotation of the tool is neglected and a snapshot in the middle of the machining process is assumed for the geometry of the simulation. The solid boundaries are fixed, one of the inserts is engaged with the work piece, but coolant is flowing over the surface. This state could estimate the distribution of the coolant in the working area for the moment when operation is paused in a middle stage, but coolant is still flowing. Figure 17 shows the geometry, computational grid, and results for impingement of the coolant jet around the working area.

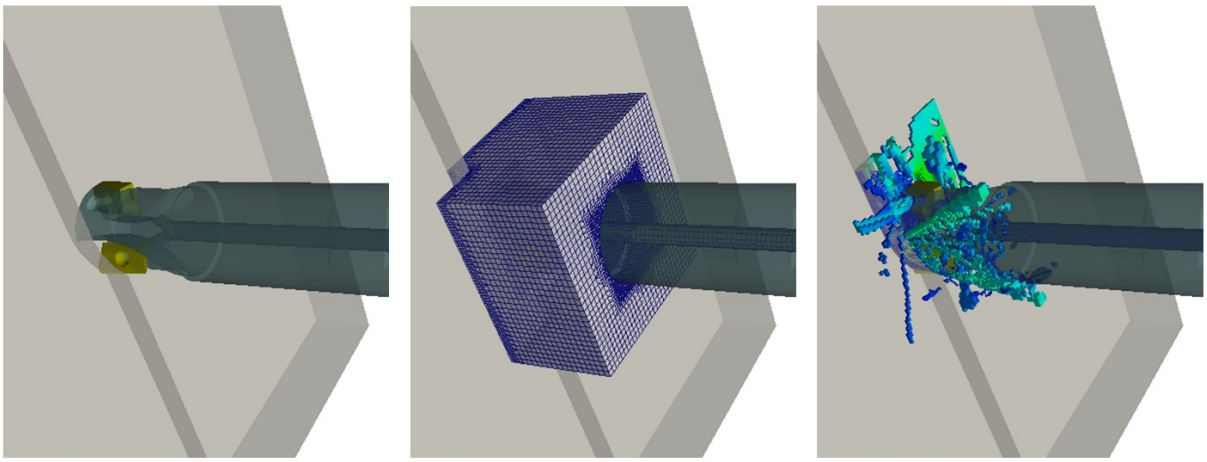

Figure 17 Steps for simulating the interaction of coolant with the cutting region. Geometry, computational grid, and sample of the results for distribution of the liquid jet around the cutting zone

Like previous studies in this paper, various simulations with different pressure setups are performed to estimate the role of coolant pressure on the jet impingement. In Figure 18, the results for the distribution of the liquid jet and the velocity contour over a plane tangential to the insert surface are displayed. Like previous simulations, by raising the coolant pressure, the velocity of the jet increased significantly, but as presented in the above row of the Figure 18, in the studies with lower pressure, the amount of the liquid which settled around the working region is higher. This observation could be an advantage for cooling with lower pressure cryogenic coolants to maximize the surface cooling with evaporation of the coolant around the working area. Among the previous studies, although referring to another application (conventional drilling), Oezkaya [30] observed that pressure/flow increments did not lead to a better cutting performance.

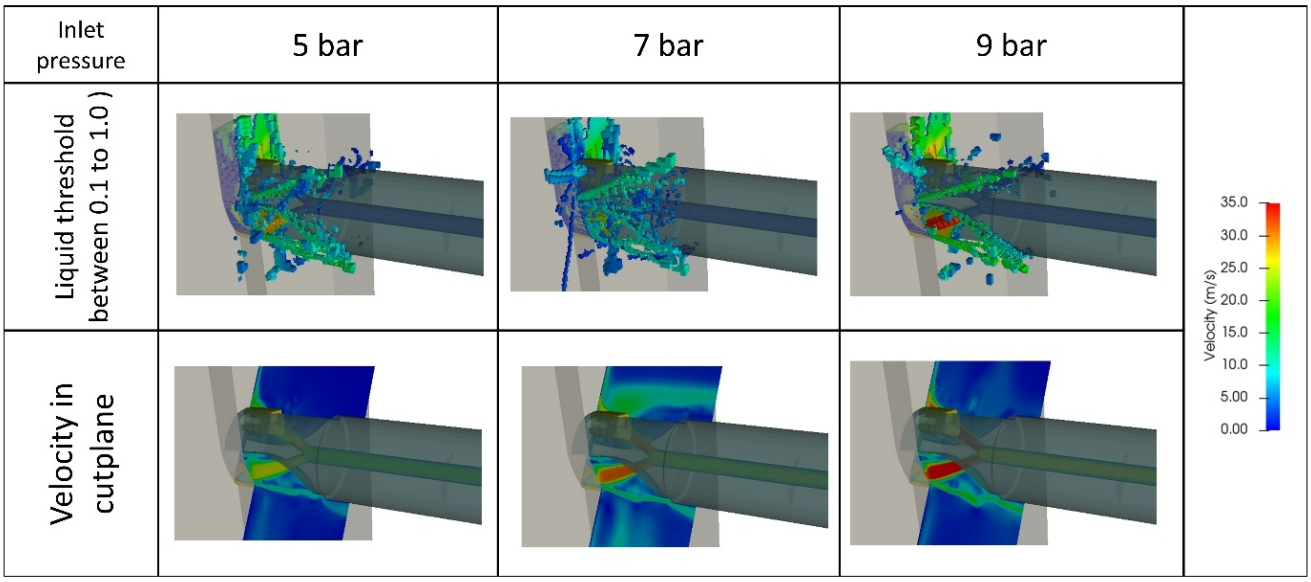

Figure 18 Results for the distribution of the coolant in the cutting region. Comparison of the simulations with different coolant pressures are presented here.

These results could be used to optimize the flow rate as well as jet orientation and to find the critical regions inside the system. Moreover, the results of the distribution of the coolant over the cutting surface could be used as a boundary condition for analyzing the heat transfer and temperature distribution during machining in cutting inserts and work piece.

According to the specific literature, an estimate of the heat transfer coefficient is far from feasible. In order to overcome this limitation, the papers dealing with the Finite Element Model FEM of machining processes typically use an iterative calibration procedure to estimate this coefficient [57][58][59]. An analysis of the conjugate heat transfer in the cutting region, mostly due evaporation of the cryogenic coolant over the surface, requires extensive studies with detailed information about the heat flux in the solid parts and the coolant distribution over the surface. The results of this paper provide adequate information about the distribution of the coolant in cutting area, which could be coupled with a FEM analysis in the future to provide a reliable heat transfer analysis.

7. Experimental verification of the numerical findings and critical discussion

To verify the numerical findings that suggest using the coolant pressure in the range of 2-4 bar at tool inlet to enhance the efficiency of the cryogenic cooling, a specific experimental campaign based on milling tests on the Ti6Al4V was carried out. The cutting tests were conceived in order to analyze the effects of the cooling condition on the mechanisms involved in milling. For this purpose, three different conditions were tested: dry cutting, cryogenic cutting with a low-pressure (p = 2.5bar) LN_2 delivery, and cryogenic cutting with a high-pressure setting for the coolant (p = 8bar). These cryogenic cuttings reproduce the conditions at the boundary of the pressure range

used for the CFD simulations, as seen in Figure 16, Figure 17, and Figure 18. Dry cutting was considered as the reference case used to determine the role of different cryogenic cooling approaches.

According to the scheme reported in Figure 19, the main idea was to exploit the cutting force measurements for identifying the unknown parameters of a mechanistic cutting model (Altintas [60]) that is typically used to analyze the mechanisms involved in cutting: shear deformation and friction between the chip and the inserts. Indeed, repeating the procedure for each tested cooling condition allowed inferences about the effect of the cryogenic cooling and the role of the liquid nitrogen pressure on these mechanisms.

Basically, the devised verification strategy is based on the comparison of the identified cutting coefficients with those obtained from dry cutting. If the identified cutting coefficients for low-pressure cryogenic cutting show higher differences with respect to dry cutting than the coefficients identified at high pressure, the CFD findings can be considered verified. Indeed, this would confirm the hypothesis that machining with a high-pressure cryogenic coolant is not as efficient as working with a low-pressure LN_2 delivery.

For the sake of generality, even a proper analysis of the chip morphology was performed to compare the effects of different cooling strategies.

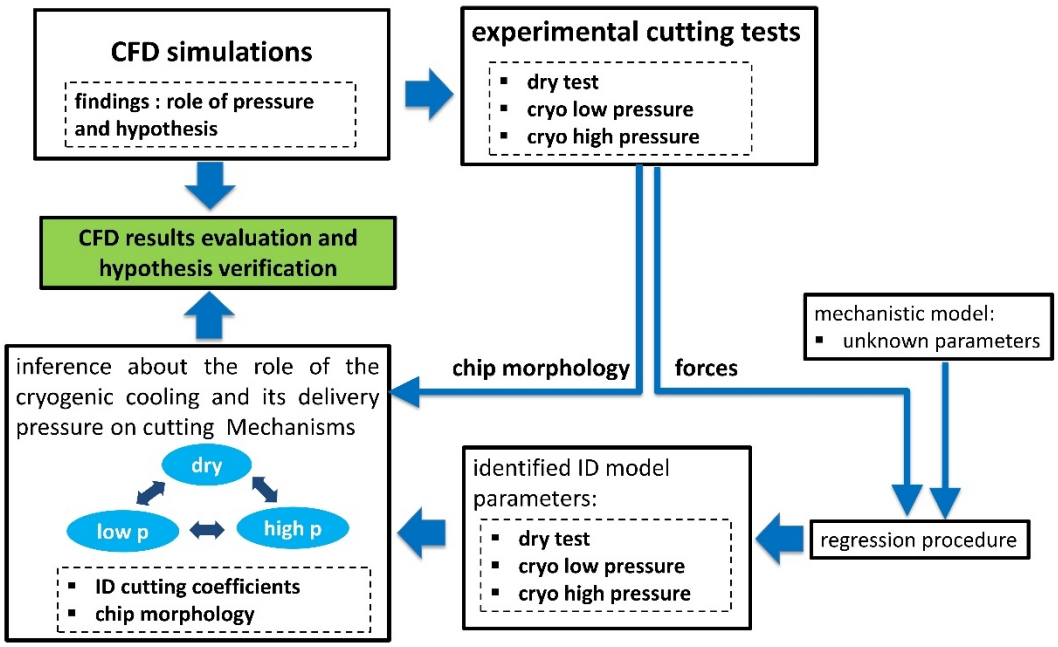

Figure 19 Numerical findings verification process

7.1. Mechanistic cutting force model to interpret the experimental results

According to the representation of a generic peripheral milling operation reported in Figure 20, the selected mechanistic model is described by equations (4-6). This formulation (Altintas [60]) is typically used to deal with vibrational issues in machining. As can be observed, the resulting

cutting force on the generic i^{th} insert/tooth engaged in the workpiece can be projected along the radial direction F_{ri}, the tangential direction F_{ti}, and the axial direction F_{ai}.

The force contributions on each insert can be computed according to equation (4).

$$\begin{aligned} F_{ti}(\varphi_i(t)) &= K_{tc} \cdot a_p \cdot h_i(\varphi_i(t)) + K_{te} \cdot a_p \\ F_{ri}(\varphi_i(t)) &= K_{rc} \cdot a_p \cdot h_i(\varphi_i(t)) + K_{re} \cdot a_p \\ F_{ai}(\varphi_i(t)) &= K_{ac} \cdot a_p \cdot h_i(\varphi_i(t)) + K_{ae} \cdot a_p \end{aligned} \quad (4)$$

K_{tc}, K_{te}, K_{rc}, K_{te}, K_{ac}, K_{ae} are the coefficients of the mechanistic model, a_p is the axial depth of cut, and h_i is the instantaneous chip thickness that varies according to the angular coordinates φ_i, equations (5) and (7).

$$h_i(\varphi_i(t)) = f_z \cdot sin\,(\varphi_i(t)) \quad (5)$$

ω is the angular tool velocity assumed constant over time t, a_e is the radial depth of cut, and f_z is the feed per tooth. These are the parameters typically set by the user before cutting.

$$A_i(\varphi_i(t)) = h_i(\varphi_i(t)) \cdot a_p \quad (6)$$

A_i is the instantaneous chip section.

$$\varphi_i(t) = \omega \cdot t \quad (7)$$

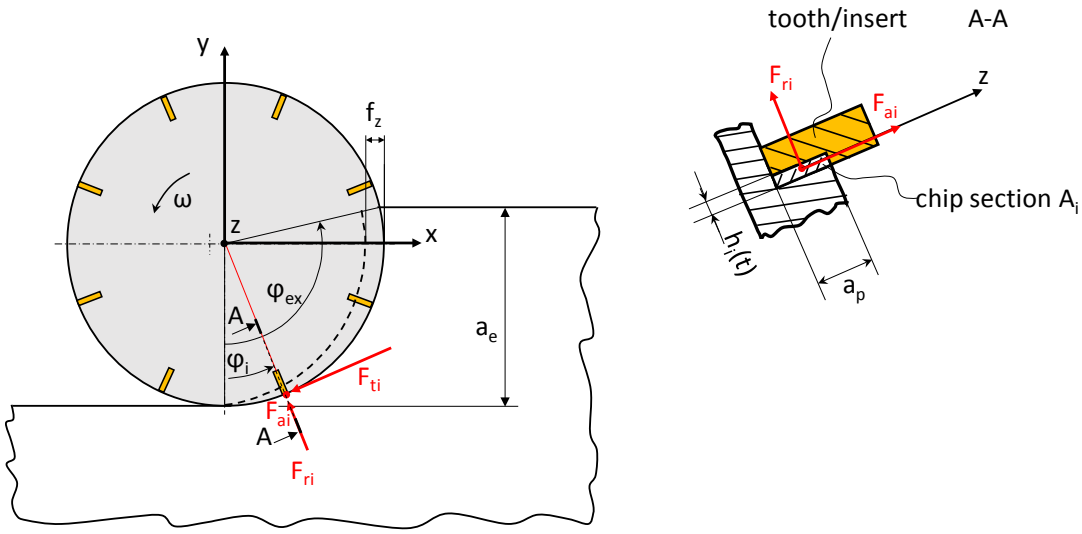

Figure 20 Milling process and representation of the cutting forces acting on a generic insert

This mechanistic force model was selected because it considers, for the computation of the main cutting force components, a contribution due to the shear (proportional to the chip section) and one linked to the friction/ploughing mechanism that, in this formulation, is considered proportional to the length of the cutting edge involved in the cutting. Since f_z is typically much lower that a_p, the length of the insert can be approximated with a_p. This formulation does not consider the tool radius.

$$A_i(\varphi_i(t)) = f_z \cdot sin\,(\varphi_i(t)) \cdot a_p \tag{8}$$

Such a simple model has the desired features for the purposes of validation. Indeed, the identification of the unknown cutting coefficients allows analyzing the main contributions to the force generation wherefore it enables inferences about the effects of the cryogenic cooling strategy on these cutting mechanisms.

7.2. Definition of tooling and cutting parameters

In order to be able to identify the unknown cutting coefficients, milling operations with different cutting parameters were carried out for each tested condition: dry, cryogenic high pressure, and cryogenic low pressure. More specifically, the feed per tooth f_z and the cutting velocity v_c were varied in random order according to Table 3. As can be observed, the combination of the considered factors (f_z – three levels, v_c – two levels) was brought to n = 6 different sets of milling parameters. The axial depth of cut was set to a_p = 3mm while the radial immersion was set to a_e = 5mm. All the cutting tests were executed in down-milling. The machine parameters, the spindle speed $\Omega = 1000 \cdot v_c/(\pi D)$, and the fee rate $V_f = f_z Z \Omega$ were even computed.

Table 3 Tested milling conditions and linked parameters

f_z [mm/tooth]	0.08	0.15	0.20	0.08	0.15	0.20
v_c [m/min]	50	50	50	70	70	70
Ω [rpm]	795.77	795.77	795.77	1114.08	1114.08	1114.08
V_f [mm/min]	127.32	238.73	318.31	178.25	334.23	445.63

The cutting tests were carried out with the tool/insert used for the CFD simulations. In greater detail, the utilized inserts were the R390-11 T3 08M-MM S30T type featuring a physical vapor deposition PVD TiAlN coating developed by Sandvik Coromant. The selected tooling is an industrial state-of-the-art solution for processing Ti6Al4V or other heat-resistant alloys HRAs.

7.3. Measurements

During the cutting tests, the cutting forces (F_x, F_y, F_z) were measured through the Kistler dynamometer 9255B with the charge amplifier type 5070A, cf. Figure 21.

The pressure at the setpoint of the tank and the pressure in the cryogenic head were also acquired. Specifically, a pressure sensor from Aplisens (PL 03-192, 0-500bar) and a pressure sensor from Gefran (TPSA E, 0-50 bar) were respectively used, see details in Figure 3. The temperature in the cryogenic head was measured with a thermocouple type K, see details on its location in Figure 3.

An example of the performed measurements is reported in Figure 22. Specifically, the cutting force measurements carried out during the milling test with LN_2 at low pressure are shown on the left (a). The right-hand side (b) displays the pressures and the temperature measurements with the high-pressure cryogenic cooling. Similar acquisitions were also performed for all the tested cooling conditions.

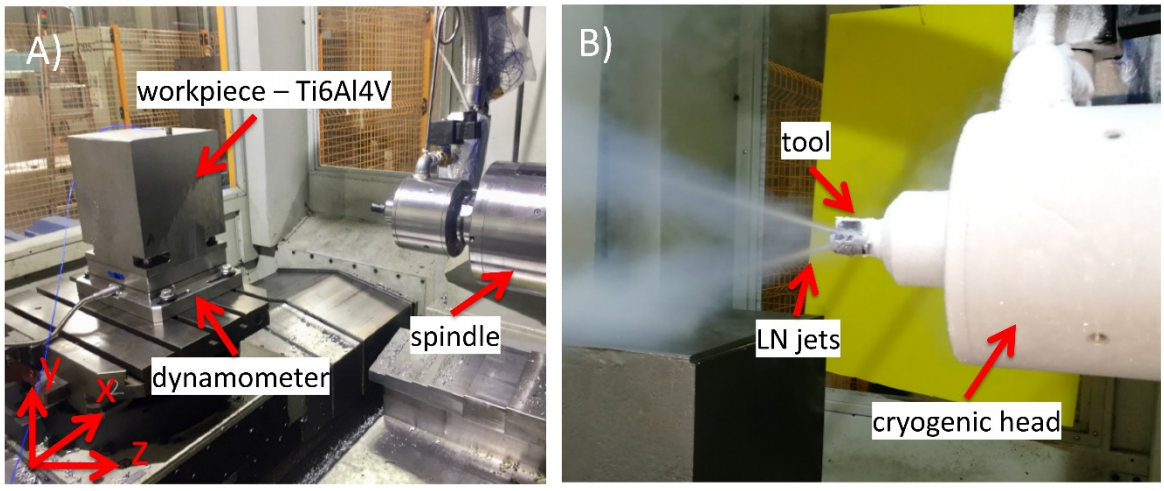

Figure 21 Experimental setup (Kistler dynamometer) and details of the cryogenic milling setup used for the validation (A), LN_2 jets (B)

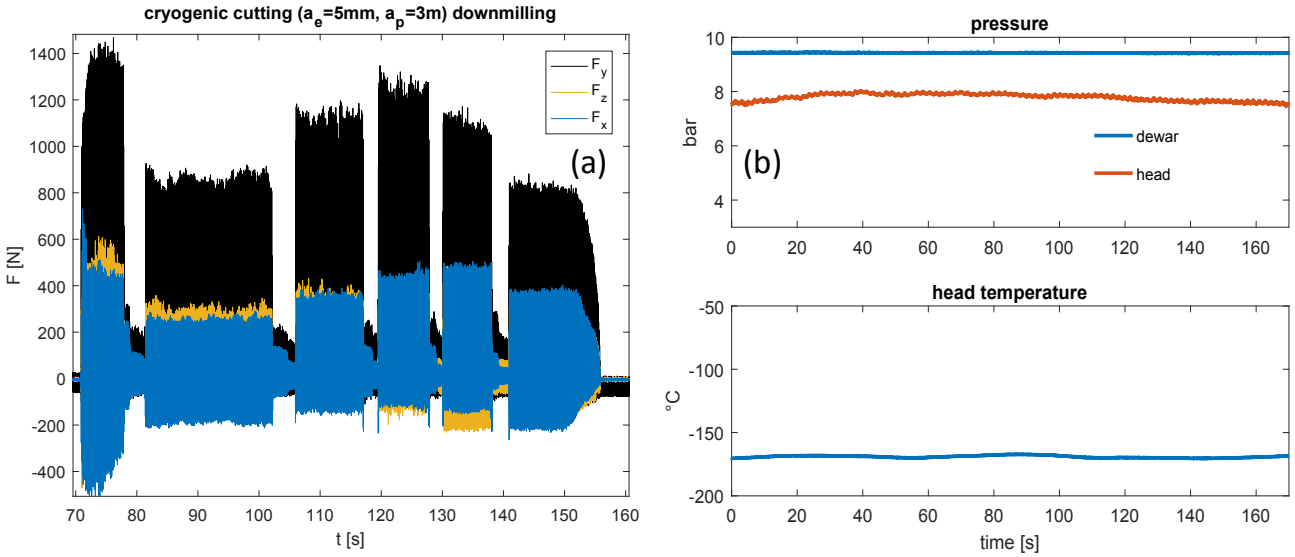

Figure 22 Example of the performed measurements: (a) cutting forces acquired during the tests carried out with the LN_2 at lower pressure; (b) pressure and temperature measurements performed during cutting tests with a high-pressure LN_2 set

Moreover, the mass flow rate was computed through differential weight measurements of the tank. Table 4 shows the summary of the pressure and temperature measurements performed during the cutting tests in different cooling conditions. Thermodynamic tables [56] show that the saturation temperature of the liquid nitrogen decreases by increasing the pressure and as it is presented in Table 4, head temperature has a lower value in low pressure test. This could be another advantage of using liquid nitrogen in low pressure regime. Furthermore, comparison of the head temperature and liquid nitrogen saturation temperature shows that cooling delivery system passed its cool-down process (section 2.1) and the coolant could cool the metal parts to very low temperature, close to the coolant liquid temperature.

Table 4 Pressure and temperature measurements (resume of the average values in different cooling conditions)

quantity/condition	dry	cryo low pressure	cryo high pressure
$\dot{m}\ [kg/h]$	-	65	95
$P_{dewar}[bar]$	-	3.5	9.42
$P_{head}[bar]$	-	2.45	7.5
$T_{head}[K]$	295	92	103
liquid nitrogen temperature [56]	-	87	99

In addition, the chips were collected during the cutting tests in all the experimented cooling conditions.

7.4. Regression procedure

The identification of the cutting coefficients is typically performed by exploiting experimental cutting force measurements, through a linear regression procedure, Montgomery [61]. Since only the cutting force along the main machine axis direction can be experimentally measured ($F_x(t)$, $F_y(t)$ and $F_z(t)$) through a force dynamometer, the linked average contributions ($\overline{F_x}$, $\overline{F_y}$, $\overline{F_z}$) can be analytically formulated via equation (9) [60].

$$\begin{aligned}
\overline{F_x} &= \left\{ \frac{Z \cdot a_p \cdot f_z}{8\pi} \cdot [K_{tc} \cdot cos2\varphi_i - K_{rc}(2\varphi_i - sin2\varphi_i)] + \frac{Z \cdot a_p}{2\pi} \cdot [-K_{te} \cdot sin\,\varphi_i + K_{re} \cdot cos\varphi_i] \right\}_{\varphi_{st}}^{\varphi_{ex}} \\
\overline{F_y} &= \left\{ \frac{Z \cdot a_p \cdot f_z}{8\pi} \cdot [K_{tc} \cdot (2\varphi_i - sin2\varphi_i) + K_{rc} cos2\varphi_i] - \frac{Z \cdot a_p}{2\pi} \cdot [K_{te} \cdot cos\,\varphi_i + K_{re} \cdot sin\varphi_i] \right\}_{\varphi_{st}}^{\varphi_{ex}} \\
\overline{F_z} &= \frac{Z \cdot a_p}{2\pi} \cdot [-K_{ac} \cdot f_z \cdot cos\varphi_i + K_{ae} \cdot \varphi_i]_{\varphi_{st}}^{\varphi_{ex}}
\end{aligned} \tag{9}$$

φ_{st} and φ_{ex} are respectively the start and exit immersion angles, and D is the tool diameter. For the analyzed milling operation, they can be computed using equation (10).

$$\begin{aligned}
&\varphi_{st} = 0;\ \varphi_{ex} \\
&\varphi_{ex} = acos\left(1 - \frac{2a_e}{D}\right)
\end{aligned} \tag{10}$$

According to the multiple linear regression theory (Montgomery [61]), the unknown cutting force coefficients $\boldsymbol{\beta} = \{K_{tc}\, K_{rc}\, K_{ac}\, K_{te}\, K_{re}\, K_{ae}\}$ can be estimated. The identified coefficients both in dry and cryogenic cooling conditions were summarized in Table 5. Moreover, in multi-regression theory (Montgomery [61]), the confidence interval $(1-\alpha)$ of the generic element $\widehat{\beta_q}$ of $\hat{\boldsymbol{\beta}}$ can be estimated. A good fitting is suggested by R^2 and R^2_{adj} that both are higher than 0.991 for all the regressions.

This is also confirmed by Figure 23 that shows, for all the tested cooling conditions, the average cutting force data (F_x, F_y and F_z) and the regression curves (F_{xfit}, F_{yfit} and F_{zfit}). For the sake of completeness, for each fitting curve, even the 95% confidence interval on the mean is presented (dotted and dashed-dotted lines) [61]. It can be observed that for low pressure cryogenic cutting, wider confidence intervals were generated.

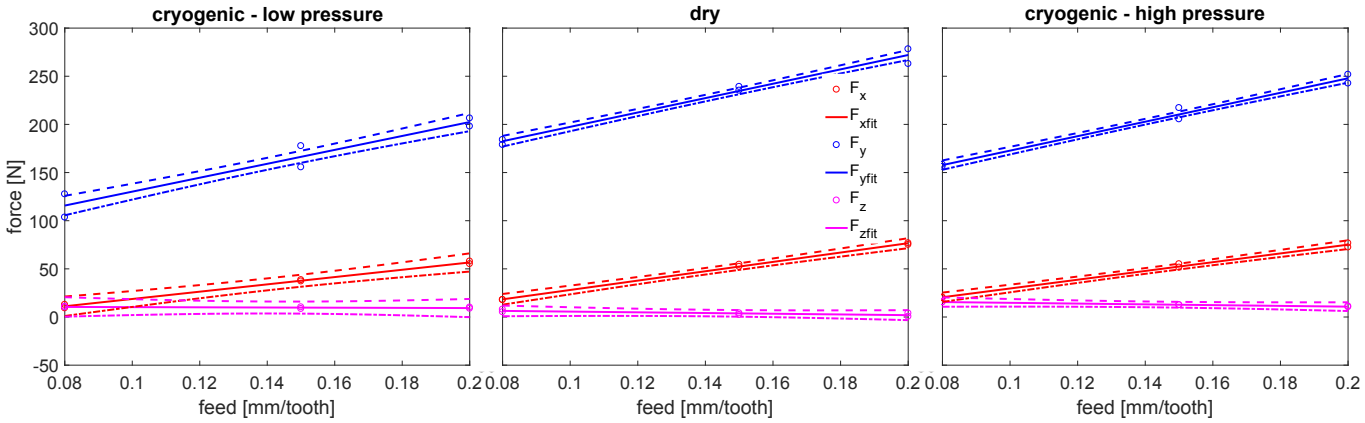

Figure 23 Experimental average force data and fitting curves – 95% confidence interval of the mean estimation

Table 5 Identified cutting coefficients in different cooling conditions

cutting coefficients $\hat{\beta}_q$	cryo low pressure	dry cutting	cryo high pressure
$\hat{K}_{tc}$ [MPa]	1623.1	1868.3	1788.40
$\hat{K}_{rc}$ [MPa]	688.9	671.5	632.20
$\hat{K}_{ac}$ [MPa]	-20.6	-99.8	-83.49
$\hat{K}_{te}$ [N/mm]	12.9	44.4	36.74
$\hat{K}_{re}$ [N/mm]	62.6	115.8	96.90
$\hat{K}_{ae}$ [N/mm]	11.2	11.7	18.72

7.5. Results and discussion

According to the procedure described in Figure 19, the verification of the CFD numerical findings was carried out comparing the identified cutting coefficients for the tested cooling conditions. The analysis was focused mainly on the cutting coefficients (K_{tc}, K_{rc}, K_{te}, K_{re}) linked to the forces in the plane X-Y that are more relevant even for the cutting power computation.

Figure 24 shows the comparisons of the shear coefficients both along the tangential (K_{tc} (a)) and radial (K_{rc} (b)) directions for the three tested cooling conditions. It can be clearly observed, even considering the 95% confidence intervals for all the parameter estimations, that the role of the cooling condition is strongly visible in K_{tc} while it can be considered negligible in K_{rc}. This is even confirmed by the 2-sample t test performed on the data, as per [61].

More specifically, for the purpose of validating the CFD findings, it is worth noting that the identified K_{tc} (for high-pressure cryogenic cutting) is close to the K_{tc} associated with dry cutting while, for low-pressure cryogenic cooling, the tangential shear coefficient is considerably lower.

This confirms that the efficiency of the cooling action is reduced by increasing the LN_2 pressure. From the phenomenological perspective, it can be assumed that the liquid nitrogen, cooling the chips, renders them more fragile. For this reason, the chip is damaged faster, and the energy required for cutting is lower. This is confirmed by the lower K_{tc} during low-pressure cryogenic cutting. Said phenomenon is not so evident when the coolant pressure is higher.

The same trend was also observed dealing with the cutting coefficients (K_{te} and K_{re}) that consider the friction between the insert and the chips. In this case, the effect is clearly visible even considering the radial direction. It was also confirmed by the hypothesis test performed on both the coefficients. Although some previous research on cryogenic machining [62] already observed a reduction of the friction coefficients compared to dry cutting, no one had studied the effects of the pressure of the coolant. It was supposed that the friction reduction is due to the formation of a LN_2 cushion [63] that penetrates between the chip and the inserts. According to the obtained results, it is most likely that this cushion does not efficiently penetrate if the coolant pressure is increased.

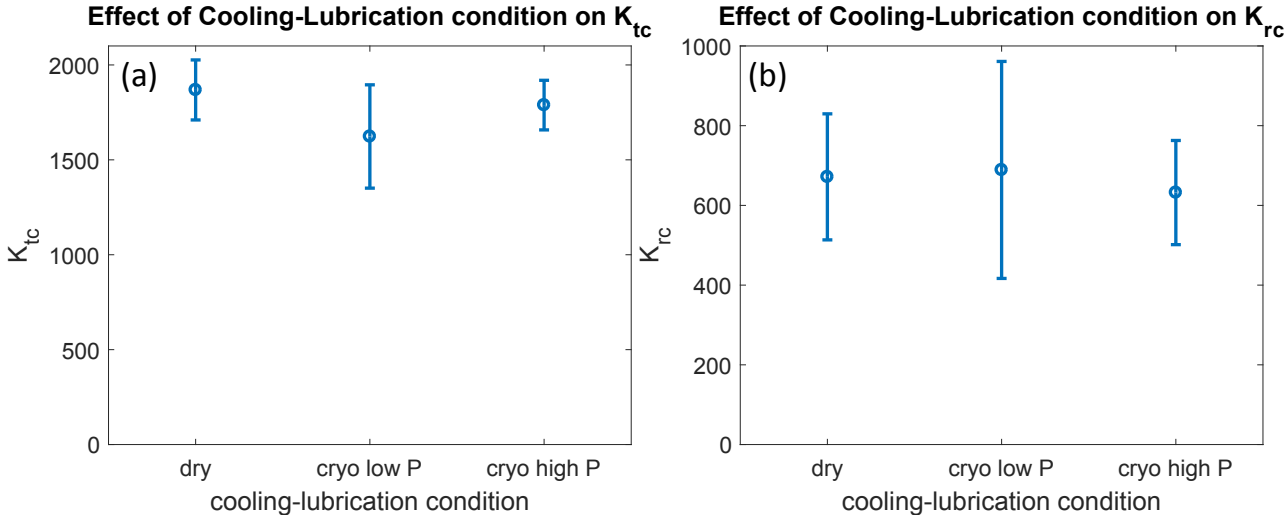

Figure 24 Estimated K_{tc} (a) and K_{rc} (b) coefficients in different cooling conditions. The 95% confidence intervals are also displayed

The chip morphology analysis (Figure 26) confirmed that the chip derived from high-pressure cryogenic cutting seems like that obtained during dry cutting. On the contrary, the chip obtained in low-pressure cryogenic milling is clearly damaged. This is in accordance with the consideration that the low-pressure cryogenic jet is capable of better cooling the chip, thus making it more fragile and more likely to be damaged. Even the wider confidence intervals (low-pressure cryogenic cooling) observed for the identified coefficients fit this assumption.

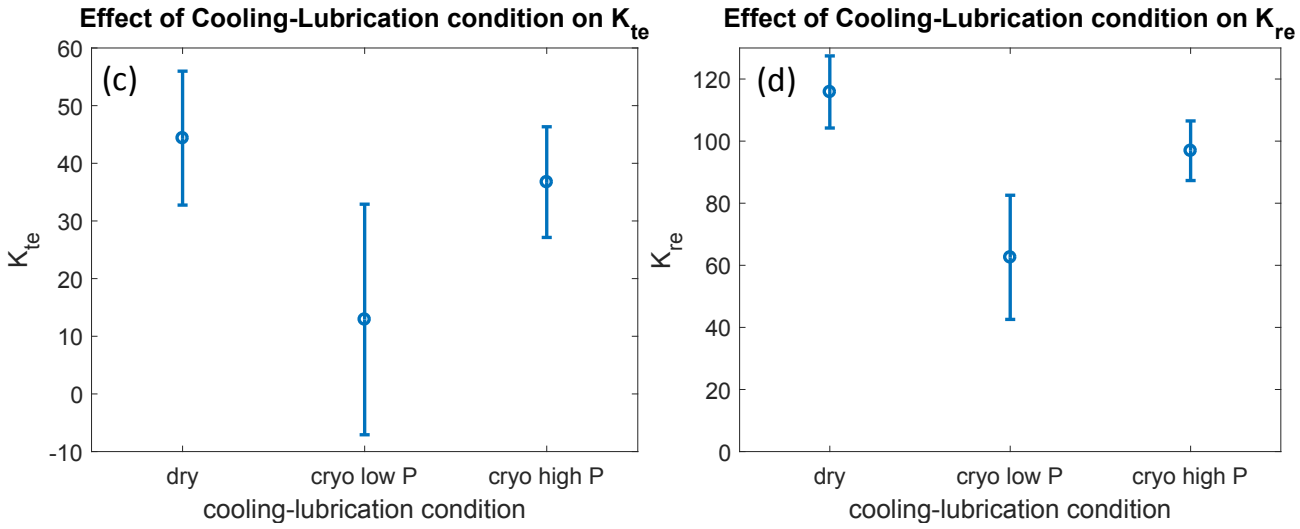

Figure 25 Estimated K_{te} (c) and K_{re} (d) coefficients in different cooling conditions. The 95% confidence intervals are also shown

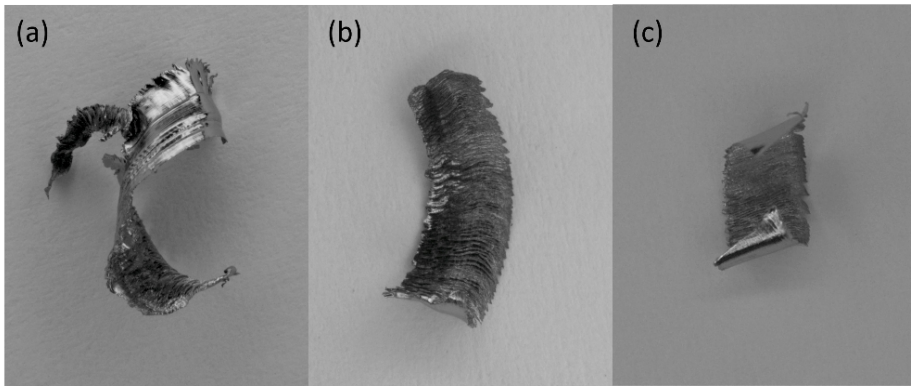

Figure 26 Chip morphology comparison (v_c = 50m/min, f_z = 0.15mm/tooth) (a) cryogenic low pressure (b) dry (c) cryogenic high pressure

Conclusions

In this paper, issues facing the cooling process of the cryogenic milling were defined briefly. Adequate analyses were implemented to learn about the performance of the coolant flow inside the coolant feeding system and then the interaction of the cryogenic coolant with milling inserts and machining area. The role of coolant pressure, milling head temperature, and coolant phase was investigated with proper simulations on different sectors. The results of this comprehensive study

can be concluded with these suggestions for development of the cryogenic milling for industrial applications.

It was found that both improving the insulation of the feeding line and finding technical solutions to insulate the non-insulated devices reduce cryogenic coolant waste during the cool-down process and consequently increase the liquid quality inside the cooling line which in turn improves the hydraulic and cooling performance of the cooling system.

The difference of the coolant flow rate, measured from both experimental tests and simulation results, for the milling tool shows that the experimental flow rate is significantly lower than the simulation with an assumption of 100% liquid at the tool entrance. Therefore, increasing the liquid quality when entering the milling tool is a crucial factor in maintaining a reliable and constant flow rate for cryogenic cooling. Improving the insulation, reducing the local pressure losses, and suitable techniques like using gas separators and sub coolers could be a solution for this issue. Using cryogenic coolant at lower pressures, in the range of 2 to 4 bar, shows benefits for the cooling process with promising results for efficient cooling: lower coolant consumption rate, higher flow transfer efficiency, and confident evaporation of the cryogenic coolant over the demanded area (inserts and cutting zone) regarding the low-speed coolant flow. A proper experimental verification based on milling tests was performed. The analysis of the cutting forces and the morphology of the chips helped interpreting the role of the coolant on cutting mechanisms. It was verified that cutting with a low-pressure cryogenic jet allows better performance than working with a high-pressure cryogenic coolant.

References

[1] D.A. Stephenson, J.S. Agapiou, Metal Cutting Theory and Practice, Boca Raton: CRC Press, 2016.

[2] A. Krämer, F. Klocke, H. Sangermann, D. Lung, Influence of the lubricoolant strategy on thermo-mechanical tool load, CIRP J. Manuf. Sci. Technol. 7 (2014) 40–47. doi:10.1016/J.CIRPJ.2013.09.001.

[3] D. Niederwestberg, B. Denkena, Simulation of thermal and mechanical workpiece load, CIRP J. Manuf. Sci. Technol. 7 (2014) 315–323. doi:10.1016/J.CIRPJ.2014.07.004.

[4] Y. Yildiz, M. Nalbant, A review of cryogenic cooling in machining processes, Int. J. Mach. Tools Manuf. 48 (2008) 947–964. doi:10.1016/j.ijmachtools.2008.01.008.

[5] M. Strano, E. Chiappini, S. Tirelli, P. Albertelli, M. Monno, Experimental evaluation of innovative tools for Ti-6Al-4V turning, 16th ESAFORM Conf. Mater. Forming, ESAFORM 2013. 554–557 (2013) 1941–1952. doi:10.4028/www.scientific.net/KEM.554-557.1941.

[6] K. Gupta, R.F. Laubscher, Sustainable machining of titanium alloys: A critical review, Proc. Inst. Mech. Eng. Part B J. Eng. Manuf. 231 (2017) 2543–2560.

doi:10.1177/0954405416634278.

[7] G. Krishnamurthy, S. Bhowmick, W. Altenhof, A.T. Alpas, Increasing efficiency of Ti-alloy machining by cryogenic cooling and using ethanol in MRF, CIRP J. Manuf. Sci. Technol. 18 (2017) 159–172. doi:10.1016/J.CIRPJ.2017.01.001.

[8] A.D. Jayal, F. Badurdeen, O.W. Dillon, I.S. Jawahir, Sustainable manufacturing: Modeling and optimization challenges at the product, process and system levels, CIRP J. Manuf. Sci. Technol. 2 (2010) 144–152. doi:10.1016/J.CIRPJ.2010.03.006.

[9] F. Pusavec, P. Krajnik, J. Kopac, Transitioning to sustainable production – Part I: application on machining technologies, J. Clean. Prod. 18 (2010) 174–184. doi:https://doi.org/10.1016/j.jclepro.2009.08.010.

[10] S. Isakson, M.I. Sadik, A. Malakizadi, P. Krajnik, Effect of cryogenic cooling and tool wear on surface integrity of turned Ti-6Al-4V, Procedia CIRP. 71 (2018) 254–259. doi:10.1016/J.PROCIR.2018.05.061.

[11] M.I. Sadik, S. Isakson, A. Malakizadi, L. Nyborg, Influence of Coolant Flow Rate on Tool Life and Wear Development in Cryogenic and Wet Milling of Ti-6Al-4V, Procedia CIRP. 46 (2016) 91–94. doi:10.1016/J.PROCIR.2016.02.014.

[12] S.Y. Hong, I. Markus, W. Jeong, New cooling approach and tool life improvement in cryogenic machining of titanium alloy Ti-6Al-4V, Int. J. Mach. Tools Manuf. 41 (2001) 2245–2260. doi:https://doi.org/10.1016/S0890-6955(01)00041-4.

[13] M. Mia, N.R. Dhar, Influence of single and dual cryogenic jets on machinability characteristics in turning of Ti-6Al-4V, Proc. Inst. Mech. Eng. Part B J. Eng. Manuf. 0 (2017) 1–16. doi:10.1177/0954405417737581.

[14] N.S.M. El-Tayeb, T.C. Yap, P.V. Brevern, Wear characteristics of titanium alloy Ti54 for cryogenic sliding applications, Tribol. Int. 43 (2010) 2345–2354. doi:10.1016/J.TRIBOINT.2010.08.012.

[15] O. Pereira, G. Urbikain, A. Rodríguez, A. Fernández-Valdivielso, A. Calleja, I. Ayesta, L.N.L. de Lacalle, Internal cryolubrication approach for Inconel 718 milling, Procedia Manuf. 13 (2017) 89–93. doi:10.1016/J.PROMFG.2017.09.013.

[16] O. Pereira, A. Rodríguez, A.I. Fernández-Abia, J. Barreiro, L.N. López de Lacalle, Cryogenic and minimum quantity lubrication for an eco-efficiency turning of AISI 304, J. Clean. Prod. 139 (2016) 440–449. doi:10.1016/J.JCLEPRO.2016.08.030.

[17] O. Pereira, A. Rodríguez, I. Ayesta, J.B. García, I.A. Fernández-Abia, L.N. Lopez De Lacalle, A cryo lubri-coolant approach for finish milling of aeronautical hard-to-cut materials, Int. J. Mechatronics Manuf. Syst. 9 (2016) 370–384.

[18] M. Nalbant, Y. Yildiz, Effect of cryogenic cooling in milling process of AISI 304 stainless steel, Trans. Nonferrous Met. Soc. China. 21 (2011) 72–79. doi:10.1016/S1003-6326(11)60680-8.

[19] D. Biermann, M. Heilmann, Improvement of workpiece quality in face milling of aluminum alloys, J. Mater. Process. Technol. 210 (2010) 1968–1975.

doi:10.1016/J.JMATPROTEC.2010.07.010.

[20] A. Shokrani, V. Dhokia, S.T. Newman, Environmentally conscious machining of difficult-to-machine materials with regard to cutting fluids, Int. J. Mach. Tools Manuf. 57 (2012) 83–101. doi:10.1016/j.ijmachtools.2012.02.002.

[21] A. Shokrani, V. Dhokia, P. Muñoz-Escalona, S.T. Newman, State-of-the-art cryogenic machining and processing, Int. J. Comput. Integr. Manuf. 26 (2013) 616–648. doi:10.1080/0951192X.2012.749531.

[22] A. Shokrani, V. Dhokia, S.T. Newman, Energy conscious cryogenic machining of Ti-6Al-4V titanium alloy, Proc. Inst. Mech. Eng. Part B J. Eng. Manuf. 232 (2018) 1690–1706. doi:10.1177/0954405416668923.

[23] A. Shokrani, V. Dhokia, S.T. Newman, Investigation of the effects of cryogenic machining on surface integrity in CNC end milling of Ti–6Al–4V titanium alloy, J. Manuf. Process. 21 (2016) 172–179. doi:10.1016/J.JMAPRO.2015.12.002.

[24] M. Strano, E. Chiappini, S. Tirelli, P. Albertelli, M. Monno, Comparison of Ti6Al4V machining forces and tool life for cryogenic versus conventional cooling, Proc. Inst. Mech. Eng. Part B J. Eng. Manuf. 227 (2013) 1403–1408. doi:10.1177/0954405413486635.

[25] S. Tirelli, E. Chiappini, M. Strano, M. Monno, Q. Semeraro, Economical Comparison of Cryogenic Vs . Traditional Turning of Ti-6Al- 4V : a Case Study, in: Key Eng. Mater. - Proceeding Esaform, Graz, 2015: pp. 1204–1210. doi:10.4028/www.scientific.net/KEM.651-653.1204.

[26] A. Davoudinejad, E. Chiappini, S. Tirelli, M. Annoni, M. Strano, FE simulation and validation of chip formation and cutting forces in dry and cryogenic cutting of Ti – 6Al – 4V, Procedia Manuf. 1 (2015). doi:10.1016/j.promfg.2015.09.037.

[27] F. Pusavec, T. Lu, C. Courbon, J. Rech, U. Aljancic, J. Kopac, I.S. Jawahir, Analysis of the influence of nitrogen phase and surface heat transfer coefficient on cryogenic machining performance, J. Mater. Process. Technol. 233 (2016) 19–28. doi:10.1016/J.JMATPROTEC.2016.02.003.

[28] F. Fallenstein, J.C. Aurich, CFD based Investigation on Internal Cooling of Twist Drills, Procedia CIRP. 14 (2014) 293–298. doi:10.1016/J.PROCIR.2014.03.112.

[29] K.S. Woon, G.L. Tnay, M. Rahman, S. Wan, S.H. Yeo, A computational fluid dynamics (CFD) model for effective coolant application in deep hole gundrilling, Int. J. Mach. Tools Manuf. 113 (2017) 10–18. doi:10.1016/J.IJMACHTOOLS.2016.11.008.

[30] E. Oezkaya, N. Beer, D. Biermann, Experimental studies and CFD simulation of the internal cooling conditions when drilling Inconel 718, Int. J. Mach. Tools Manuf. 108 (2016) 52–65. doi:10.1016/J.IJMACHTOOLS.2016.06.003.

[31] M.S. Najiha, M.M. Rahman, A computational fluid dynamics analysis of single and three nozzles minimum quantity lubricant flow for milling, Int. J. Automot. Mech. Eng. 10 (2014) 1891–1900. doi:10.15282/ijame.10.2014.6.0157.

[32] C. Tahri, P. Lequien, J.C. Outeiro, CFD Simulation and Optimize of LN2 Flow Inside Channels Used for Cryogenic Machining: Application to Milling of Titanium Alloy Ti-6Al-4V, Procedia CIRP. 58 (2017) 584–589. doi:10.1016/J.PROCIR.2017.03.230.

[33] Randall F. Barron, Gregory F. Nellis, CryogeniC Heat transfer, 2016.

[34] S. Chandra, Leidenfrost Evaporation of Liquid Nitrogen Droplets, 116 (2016) 999–1006.

[35] L. Qiu, S. Dubey, F. Hoong, F. Duan, International Journal of Heat and Mass Transfer Recent developments of jet impingement nucleate boiling, Int. J. Heat Mass Transf. 89 (2015) 42–58. doi:10.1016/j.ijheatmasstransfer.2015.05.025.

[36] I. Starodubtseva, A. Pavlenko, The Evolution of Temperature Disturbances During Boiling of Cryogenic Liquids on Heat-Releasing Surfaces, (2014). doi:10.5772/23684.

[37] D.T. Vader, F.P. Incropera, R. Viskanta, Convective Nucleate Boiling on a Heated Surface Cooled by an Impinging , Planar Jet of Water, (2018).

[38] K.D. Timmerhaus, T.M. Flynn, Cryogenic Process Engineering, International Cryogenics Monograph Series, 1989.

[39] V.P. Carey, Liquid Vapor Phase Change Phenomena: An Introduction to the Thermophysics of Vaporization and Condensation Processes in Heat Transfer Equipment, second edi, 2007.

[40] I. Mamoru, H. Takashi, Thermo-Fluid Dynamics of Two-Phase Flow, 2011.

[41] G.F. Hewitt, N.S. Hall-Taylor, Annular Two-Phase Flow, 1970.

[42] J.C. Rozzi, J.K. Sanders, C.H. Passow, M.P. Day, W.M. Fischer, Device for Axial Delivery of Cryogenic Fluids Through a Machine Spindle, US20100272530A1, 2009.

[43] J.C. Rozzi, J.K. Sanders, N.W. Brown, M.P. Day, Mechanism for delivering cryogenic coolant to a rotating tool, US8777529B2, 2010.

[44] J.P. Franc, J.M. Michel, Fundamentals of Cavitation, Kluwer Academic Publishers, 2010.

[45] E. Tahmasebi, P. Albertelli, T. Lucchini, Recent Advances in Simulation of Flow in Cryogenic Cooling for Hard-to-Cut Materials, in: 14th Int. Conf. High Speed Mach., San Sebastian (Spain), 2018.

[46] Y. Sun, Z. Guan, K. Hooman, Cavitation in Diesel Fuel Injector Nozzles and its Influence on Atomization and Spray, Chem. Eng. Technol. (2018) 6–29. doi:10.1002/ceat.201800323.

[47] E. Tahmasebi, T. Lucchini, G. D'Errico, A. Onorati, G. Hardy, An investigation of the validity of a homogeneous equilibrium model for different diesel injector nozzles and flow conditions, Energy Convers. Manag. 154 (2017) 46–55. doi:10.1016/J.ENCONMAN.2017.10.049.

[48] E. Tahmasebi, T. Lucchini, G. D'Errico, A. Onorati, Numerical Simulation of Diesel Injector Internal Flow Field, Energy Procedia. 82 (2015) 51–58. doi:10.1016/J.EGYPRO.2015.11.882.

[49] F.J. Salvador, J. Martínez-López, M. Caballer, C. De Alfonso, Study of the influence of the needle lift on the internal flow and cavitation phenomenon in diesel injector nozzles by CFD using RANS methods, Energy Convers. Manag. 66 (2013) 246–256. doi:10.1016/J.ENCONMAN.2012.10.011.

[50] D.P. Schmidt, M.-L. Corradini, A Fully compressible, two-dimensional model of small, high-speed, cavitating nozzels, At. Sprays. 9 (1999) 255–276.

[51] C. Habchi, N. Dumont, O. Simonin, Multidimensional simulation of cavitating flows in diesel injectors by a homegeneous mixture modeling approach, At. Sprays. 18 (2008) 129–162.

[52] E. Tahmasebi, Simulation of internal flow in fuel injection process, Politecnico di Milano, 2016.

[53] S.S. Deshpande, L. Anumolu, M.F. Trujillo, Evaluating the performance of the two-phase flow solver interFoam, Comput. Sci. Discov. 5 (2012) 1–36. doi:10.1088/1749-4699/5/1/014016.

[54] H. Jasak, A. Jemcov, Z. Tukovic, OpenFOAM: A C++ library for complex physics simulations, in: Int. Work. Coupled Methods Numer. Dyn., Dubrovnik Croatia, 2007: pp. 1–20.

[55] F.R. Menter, M. Kuntz, R. Langtry, Ten Years of Industrial Experience with the SST Turbulence Model, Turbul. Heat Mass Transfe. 4 (2003) 625–632.

[56] E.W. Lemmon, M.L. Huber, M.O. McLinden, NIST Standard Reference Database 23: Reference Fluid Thermodynamic and Transport Properties-REFPROP, in: Natl. Inst. Stand. Technol. Stand. Ref. Data Progr., 2013.

[57] G. Rotella, D. Umbrello, Finite element modeling of microstructural changes in dry and cryogenic cutting of Ti6Al4V alloy, CIRP Ann. 63 (2014) 69–72. doi:https://doi.org/10.1016/j.cirp.2014.03.074.

[58] S. Imbrogno, S. Sartori, A. Bordin, S. Bruschi, D. Umbrello, Machining Simulation of Ti6Al4V under Dry and Cryogenic Conditions, Procedia CIRP. 58 (2017) 475–480. doi:10.1016/J.PROCIR.2017.03.263.

[59] S.Y. Hong, Y. Ding, Cooling approaches and cutting temperatures in cryogenic machining of Ti-6Al-4V, Int. J. Mach. Tools Manuf. 41 (2001) 1417–1437. doi:https://doi.org/10.1016/S0890-6955(01)00026-8.

[60] Y. Altintas, Manufacturing Automation, 2012.

[61] D. Montgomery, Design and Analysis of Experiments, 5th editio, John Wiley adn Sons, 2001.

[62] I.S. Jawahir, H. Attia, D. Biermann, J. Duflou, F. Klocke, D. Meyer, S.T. Newman, F. Pusavec, M. Putz, J. Rech, V. Schulze, D. Umbrello, Cryogenic manufacturing processes, CIRP Ann. 65 (2016) 713–736. doi:10.1016/J.CIRP.2016.06.007.

[63] V.S. Sharma, M. Dogra, N.M. Suri, Cooling techniques for improved productivity in

Acknowledgement

This research was developed in the framework of the project “Nuovo processo di asportazione di truciolo supportato da fluido criogenico per materiali aeronautici di difficile lavorabilità: incremento della produttività, riduzione dei costi ed eliminazione degli oli da taglio”. The project was founded by the “Ministero dello Sviluppo Economico” and performed in Consorzio MUSP. The project involves an important Italian machine tool manufacturer, Jobs Spa that belongs to FFG group. The authors would like to thank all the Consorzio MUSP and Jobs Spa staff that collaborated to the project development. Moreover, the authors would like to thank the SIAD company for the LN_2 delivery and collaboration on the cryogenic plant enhancement.